NASA Technical Memorandum 81238

A Mathematical Model of the CH-53 Helicopter

William R. Sturgeon
James D. Phillips, Ames Research Center, Moffett Field, California

National Aeronautics and Space Administration

Ames Research Center
Moffett Field, California 94035

TABLE OF CONTENTS

SYMBOLS

A_1, B_1	lateral and longitudinal cyclic control, swashplate angle, commands
A_{1afcs}, B_{1afcs}	lateral and longitudinal cyclic AFCS control, swashplate angle, commands
A_1', B_1'	lateral and longitudinal cyclic control, swashplate angle, in shaft axes
a	rotor blade lift-curve slope
a'	small angle used to define rotor drag force
a_o	coning angle
a_1, b_1	longitudinal and lateral flapping angles in control axes
a_{1s}, b_{1s}	longitudinal and lateral flapping angles in shaft axes
a_y	lateral specific force, positive in direction of Y_h
B	rotor blade tip-loss constant
b	number of blades per rotor
C	transformation matrix from Euler angle rates to angular velocity in body axes
$C_{c/s}$	transformation matrix from shaft to control axes
$C_{h/e}$	transformation matrix from Earth to body axes
$C_{h/wt}$	transformation matrix from wind tunnel to body axes
C_Q	torque coefficient
$C_{s/h}$	transformation matrix from body to shaft axes
C_T	thrust coefficient
C_y	rotor side force coefficient
c	blade chord
D_{wt}	fuselage drag in wind-tunnel axes
e	flapping hinge offset

e_{kf}, e_{kt}	fuselage and tail angle-of-attack corrections due to main rotor downwash
e_{mr}	main rotor downwash factor
G_{gov}	gas generator governor gain
g	acceleration of gravity
H	rotor drag force
h	altitude
h_c	altitude command
I_{afcs}	integer indicating AFCS engaged
I_{ah}	integer indicating altitude-hold engaged
I_b	blade moment of inertia about flapping axis
I_h	inertia matrix of helicopter, in body axes
I_{mr}	polar moment of inertia of the main rotor
I_{ped}	integer indicating pilots feet off pedals
I_{pt}	moment of inertia of power turbine
I_{tc}	integer indicating turn coordination engaged
I_{trim}	integer indicating cyclic trim button released
I_{xlat}	integer indicating lateral cyclic stick displacement from zero force trim position
i_t	flow incidence at the horizontal tail
i_{to}	fixed incidence of the horizontal tail
J	rotor side force
K_c	main rotor shaft compliance
K_d	main rotor shaft damping
K_f	pitching moment coefficient due to main rotor thrust
K_{gov}	power turbine governor gain
K_i, i=1, 24	constant gains in control system

$[L, M, N]_{d, h}$	body axes moments due to angular velocity
$[L, M, N]_{f, h}$	body axes moments due to fuselage aerodynamics
$[L, M, N]_{hub, h}$	body axes moments due to rotor moments transmitted at the hub
$[L, M, N]_{hub, s}$	shaft axes moments due to rotor moments transmitted at the hub
$[L, M, N]_{r, h}$	total body axes moments due to the rotor
$[L, M, N]_{wt}$	body axes aerodynamic moments acting on the fuselage
$\tilde{L}_{wt}$	fuselage lift in wind-tunnel axes
M_w	mass moment of rotor blade
m	helicopter mass
$[p, q, r]_c$	angular velocities in control axes
$[p, q, r]_h$	angular velocities in body axes
$[p, q, r]_s$	angular velocities in shaft axes
Q_{am}	aerodynamic torque acting on main rotor, positive in direction opposite to rotation
Q_{at}	aerodynamic torque acting on tail rotor, positive in direction opposite to rotation
Q_{eng}	engine torque acting on the main rotor shaft and fuselage, positive value tends to accelerate main rotor and cause fuselage to yaw right
Q_{gen}	gas generator torque
Q_s	rotor shaft torque acting on the fuselage
$\bar{q}$	dynamic pressure
R	rotor radius
s	Laplace operator
T	thrust
t_o	time delay in primary servo transfer function
$[u, v, w]_{as, h}$	true airspeed of helicopter c.g. in body axes

$[u, v, w]_c$	true airspeed of rotor hub in control axes
$[u, v, w]_{cg, e}$	inertial velocity of helicopter c.g. in Earth axes
$[u, v, w]_{cg, h}$	inertial velocity of helicopter c.g. in body axes
$[u, v, w]_{gust, h}$	gust velocity in body axes
$[u, v, w]_s$	true airspeed of the rotor hub in shaft axes
$[u, v, w]_{wind, h}$	wind velocity in body axes
$V_{as, h}$	total true airspeed
X_{col}, X_{lat}, X_{lon}, X_{ped}	pilot control displacements of collective stick, lateral and longitudinal cyclic stick, and pedals from nominal positions. (Positive displacements cause climb, roll right, pitch down, and yaw left, respectively.)
$[X, Y, Z]_{f, h}$	body axis forces due to fuselage aerodynamics
$[X, Y, Z]_{r, h}$	body axis forces due to the rotor
$[x, y, z]_{cg, e}$	inertial position in Earth axes
$[x, y, z]_{ps, h}$	pilots eye location in body axes
$[x, y, z]_{r, h}$	rotor hub location in body axes
$[x, y, z]_{wt, h}$	wind-tunnel mounting point in body axes
Y_{wt}	fuselage side force in wind-tunnel axes
α_f, β_f	fuselage angle of attack and sideslip
α_{f_l}	fuselage local angle of attack
ϵ	rotor orientation angle
γ	rotor lock number, $\frac{\rho a c R^4}{I_b}$
ζ	damping ratio in primary servo transfer function
θ_{ct}	tail rotor collective pitch command
θ'_{ct}	tail rotor collective pitch
θ_{mafcs}	main rotor collective pitch AFCS command
θ_{mm}	main rotor collective pitch command

θ'_{om}	main rotor collective pitch
θ_{ot}	effective value of tail rotor collective pitch
θ_s	longitudinal shaft tilt angle
θ_{tafcs}	tail rotor collective pitch AFCS command
θ_t	blade twist angle, from root to tip
$\theta_{.75}$	blade pitch at 3/4 radius
λ	inflow ratio
μ	tip-speed ratio
ν	induced inflow ratio
ρ	atmospheric density
σ	rotor solidity, $\frac{bc}{\pi R}$
τ	time constant in primary servo transfer function
τ_{eng}	eagine time constant
τ_i, $i = 1, 8$	time constants in control system
τ_ν	inflow time constant
ϕ_{trim}	trim value of ϕ
ϕ_s	lateral shaft tilt angle
$[\phi, \theta, \psi]_h$	Euler angles, relating body and Earth axes
ψ_{trim}	trim value of ψ
ψ_{wt}	wind-tunnel yaw angle
Ω	rotor angular velocity
Ω_{pt}	power turbine angular velocity
Ω_o	commanded rotor angular velocity
ω_n	natural frequency in primary servo transfer function

Subscripts:

c	control axes
e	Earth axes
h	body axes
m	main rotor
s	shaft axes
t	tail rotor
wt	wind-tunnel axes

Superscripts:

T	matrix transpose
$(\dot{})$	time derivative of ( )

A MATHEMATICAL MODEL OF THE CH-53 HELICOPTER

William R. Sturgeon and James D. Phillips

Ames Research Center

SUMMARY

A mathematical model suitable for real-time simulation of the CH-53 helicopter is presented. This model, which is based on modified nonlinear classical rotor theory and nonlinear fuselage aerodynamics, will be used to support terminal-area guidance and navigation studies on a fixed-base simulator. Validation is achieved by comparing the model response with that of a similar aircraft and by a qualitative comparison of the handling characteristics made by experienced pilots.

INTRODUCTION

Terminal-area guidance and navigation helicopter research is to be conducted at Ames Research Center. Prior to actual flight tests, advanced concepts and procedures will be evaluated using a piloted flight simulator. This simulator facility consists of a "fixed-base" cockpit, configured to that of the CH-53 (fig. 1), and a Sigma 9 digital computer. Operation of this simulator requires the use of a CH-53 mathematical model that can operate in real time on the Sigma 9 host computer.

Helicopter models range in complexity from linear models, which are valid near one particular flight condition, to nonlinear blade-element models which account for complex rotor flow conditions and are used over the entire flight regime. A model of intermediate complexity, which meets simulation requirements for terminal-area guidance and navigation studies, is based on quasi-static rotor representations. A CH-53 model of this latter type is presented.

The help of the following persons in obtaining this mathematical model is acknowledged: Dean E. Cooper, Thomas H. Lawrence, and Phil Gold of Sikorsky Aircraft Division of United Technologies, Stratford, Connecticut; and J. D. Shaughnessy of Langley Research Center. The model was programmed on the Sigma 9 computer by Boris Voh of Computer Science Corporation. Validation was performed with the help of George Tucker and Ron Gerdes of Ames Research Center.

MATHEMATICAL MODEL

The helicopter mathematical model is defined in terms of submodels of the fuselage aerodynamics, rotor systems, engine and governor, and control system. The relative relationship of these submodels is discussed in the section entitled "General Model Description" which precedes detailed descriptions of

each submodel. The submodels are defined in terms of forces, moments, and motion expressed in the following coordinate systems which are used in the development of the mathematical model (fig. 2).

Coordinate Systems

1. Earth axes, subscript e: Origin fixed on the Earth's surface, x_e axis pointing north, y_e pointing east (fig. 2(a)).

2. Helicopter body axes, subscript h: Origin at the center of gravity (c.g.), x_h axis forward in the plane of symmetry and parallel to the waterline, z_h axis down in the plane of symmetry (fig. 2(a)).

3. Shaft axes, subscript s: Origin at the rotor hub, x_s axis rotated through the longitudinal shaft tilt angle θ_s about the y_h axis, y_s axis rotated through the lateral shaft tilt angle ϕ_s about the x_s axis, z_s axis coincident with the rotor shaft (fig. 2(b)). This applies to both the main and tail rotors.

4. Control axes, subscript c: Origin at the rotor hub, z_c axis directed toward the fuselage along the axis of no-feathering (an axis perpendicular to the swashplate), x_c axis points into the relative wind so that the y_c component of the relative wind is zero (fig. 2(c)). This applies to both the main and tail rotors.

5. Wind-tunnel axes, subscript wt: Origin at the wind-tunnel mounting point, x_{wt} axis pointing into the relative wind, z_{wt} down and perpendicular to the relative wind.

General Model Description

The helicopter model is defined in terms of the following submodels:

1. Fuselage aerodynamics model: The fuselage aerodynamics model defines nonlinear lift, drag, and side forces as well as pitching, rolling, and yawing moments in terms of a wide range of fuselage angles of attack and sideslip, rotor downwash, body angular velocity, and dynamic pressure.

2. Rotor model: nonlinear models for the main rotor and tail rotor define thrust, drag, and side forces as well as hub force and moments representative of articulated rotors over a wide range of airspeeds through hover to rearward and sideward flight. The rotor models account for variable inflow velocity, variable rotor speed, blade twist, tip loss, blade coning, blade flapping, flapping-hinge offset, and tail-rotor δ_3 hinge.

3. Engine model: An engine and governor model adapted from a heavy lift helicopter simulation provides a realistic time delay between aerodynamic rotor torque and the resulting reaction torque applied to the fuselage. The model includes the effects of gas turbine, power turbine, rotor inertia, and shaft compliance.

4. Control system model: The helicopter control system model converts pilot's cyclic control, collective control, and pedal inputs into main and tail rotor cyclic and collective pitch inputs. An automatic flight control system (AFCS) is included which provides helicopter rate and attitude stabilization in roll, pitch, and yaw.

Wind and gust inputs to the helicopter model are provided, as well as the pilot control inputs. All forces and moments acting on the helicopter are outputs of the fuselage aerodynamics and the rotor systems submodels. Fuselage forces and moments are calculated in wind-tunnel axes and transformed to body axes. Rotor forces are calculated in control axes and transformed to body axes, and the rotor moments are calculated in shaft axes and transformed to body axes.

The equations of motion use the total forces and moments, in body axes, to calculate the translational and angular body axis accelerations. The translational acceleration is integrated to give body inertial velocity which is transformed to Earth axes and integrated to obtain helicopter position. The angular acceleration is integrated to give body angular velocity, which is transformed to Euler angular velocity and integrated to obtain helicopter attitude.

The relative relationship of the submodels is shown in Figure 3(a), and the inputs and outputs of each submodel are shown in figures 3(b) through 3(g). The model parameters are given in Table 1.

Fuselage Aerodynamics

The fuselage aerodynamic data are given in both equation and tabular form. The forces and moments are given in wind-tunnel axes in terms of local angle of attack, local angle of incidence at the tail, sideslip angle, body angular velocity, and dynamic pressure.

Airspeed in body axes- The helicopter airspeed is expressed in terms of its inertial velocity and the wind velocity as

$$\begin{bmatrix} u \\ v \\ w \end{bmatrix}_{as,\,h} = \begin{bmatrix} u \\ v \\ w \end{bmatrix}_{cg,\,h} - \begin{bmatrix} u \\ v \\ w \end{bmatrix}_{gust,\,h} - \begin{bmatrix} u \\ v \\ w \end{bmatrix}_{wind,\,h} \tag{1}$$

The free-stream angle of attack and sideslip angle are defined as

$$\alpha_f = \tan^{-1}\left(\frac{w}{u}\right), \quad -\pi \le \alpha_f \le \pi \tag{2}$$

and

$$\beta_f = \sin^{-1}\left(\frac{v}{V_{as,\,h}}\right), \quad \frac{-\pi}{2} \le \beta_f \le \frac{\pi}{2} \tag{3}$$

respectively, where

$$V_{as,\,h} = \left(\sqrt{u^2 + v^2 + w^2}\right)_{as,\,h} \tag{4}$$

and the free-stream dynamic pressure is

$$\bar{q} = \frac{1}{2}\rho V_{as,\,h}^2 \tag{5}$$

Main rotor downwash effect- The effect of the main rotor downwash on the local angle of attack is accounted for by the rotor downwash factor (ref. 1):

$$e_{mr} = \frac{C_{Tm}}{2(\lambda_m^2 + \mu_m^2)} \tag{6}$$

C_{Tm}, λ_m, and μ_m are rotor parameters defined in the following section. The fuselage local angle of attack is

$$\alpha_{f\ell} = \alpha_f - e_{mr}e_{kf}, \quad -\pi \le \alpha_{f\ell} \le \pi \tag{7}$$

and the local incidence at the tail is

$$i_t = i_{to} - (e_{kt} - e_{kf})e_{mr} \tag{8}$$

where e_{kt} and e_{kf} are empirical constants. The wind-tunnel yaw angle is

$$\psi_{wt} = -\beta_f \tag{9}$$

Fuselage forces and moments in wind tunnel axes- The fuselage forces and moments in wind-tunnel axes are provided through the wind-tunnel data given in figures 4 through 13. These curves are entered with the fuselage local angle of attack (eq. (7)), local incidence at the tail (eq. (8)), wind-tunnel yaw angle (eq. (9)), and dynamic pressure (eq. (5)) as determined from the equations noted.

Since the wind-tunnel data do not cover the full range of angle of attack and sideslip, it is assumed that force and moment coefficients remain constant beyond the limits of these angles for which data are given. This assumption should not significantly degrade the model performance, for large values of the above angles generally occur at low airspeeds where fuselage forces and moments are relatively small.

The fuselage forces and moments are determined as follows:

$$D_{wt} = \left(\frac{\Delta D_{1wt}}{\bar{q}} + \frac{\Delta D_{2wt}}{\bar{q}}\right)\bar{q}$$

where

$$\frac{\Delta D_{2wt}}{\bar{q}} = 300 \sin \psi_{wt}^2 \quad (ft^2)$$

$$= 27.9 \sin \psi_{wt}^2 \quad (m^2)$$

Also,

$$\tilde{L}_{wt} = \left(\frac{\Delta \tilde{L}_{1wt}}{\bar{q}} + \frac{\Delta \tilde{L}_{2wt}}{\bar{q}}\right) \bar{q}$$

$$Y_{wt} = \left(\frac{Y_{wt}}{\bar{q}}\right) \bar{q}$$

$$L_{wt} = \left(\frac{\Delta L_{1wt}}{\bar{q}} + \frac{\Delta L_{2wt}}{\bar{q}}\right) \bar{q}$$

$$M_{wt} = \left(\frac{\Delta M_{1wt}}{\bar{q}} + \frac{\Delta M_{2wt}}{\bar{q}}\right) \bar{q}$$

$$N_{wt} = \left(\frac{N_{wt}}{\bar{q}}\right) \bar{q}$$

Transformation of fuselage aerodynamic forces to body axes- The fuselage aerodynamic forces are transformed from wind tunnel to body axes.

$$\begin{bmatrix} X \\ Y \\ Z \end{bmatrix}_{f,\ h} = C_{h/wt} \begin{bmatrix} -D \\ Y \\ -\tilde{L} \end{bmatrix}_{wt} \tag{10}$$

$$C_{h/wt} = \begin{bmatrix} \cos \alpha_f \cos \beta_f & -\cos \alpha_f \sin \beta_f & -\sin \alpha_f \\ \sin \beta_f & \cos \beta_f & 0 \\ \sin \alpha_f \cos \beta_f & -\sin \alpha_f \sin \beta_f & \cos \alpha_f \end{bmatrix}$$

Transformation of fuselage aerodynamic moments to body axes- The total fuselage aerodynamic moments include the basic wind-tunnel moments, additional moments due to the wind-tunnel mounting point being offset from the c.g., damping due to angular velocity, and rotor downwash on the tail. In body axes these moments are

$$\begin{bmatrix} L \\ M \\ N \end{bmatrix}_{f,\,h} = \begin{bmatrix} L \\ M \\ N \end{bmatrix}_{wt} + \begin{bmatrix} 0 & -z & y \\ z & 0 & -x \\ -y & x & 0 \end{bmatrix}_{wt,\,h} \begin{bmatrix} X \\ Y \\ Z \end{bmatrix}_{f,\,h} + \begin{bmatrix} L \\ M \\ N \end{bmatrix}_{d,\,h} + \begin{bmatrix} 0 \\ k_f \\ 0 \end{bmatrix} T_m \qquad (11)$$

where

$$\begin{bmatrix} L \\ M \\ N \end{bmatrix}_{d,\,h} = \begin{bmatrix} 0 & \\ -899 & q_h \\ -520 & r_h \end{bmatrix} V_{as,\,h} \qquad (12)$$

and T_m is the main rotor thrust. Both the damping equation and rotor downwash moment coefficient were obtained from an unpublished Sikorsky Aircraft report.

The inputs and outputs of the fuselage aerodynamic model are shown in figure 3(b).

Rotor Models

The rotor forces and moments are calculated using nonlinear classical rotor theory, specifically a modified Bailey representation used in reference 1 and discussed in references 2 through 5. Important aspects of this rotor model are

1. Uniform inflow over the rotor disk is assumed
2. Compressibility and stall effects are neglected
3. Lagging motion of the rotor blades is neglected
4. Only first harmonic motion of the rotor blades is considered
5. The blade coning and flapping angles are assumed quasi-static

This relatively simple rotor model is used to facilitate its use in a real-time simulation. This model is valid for forward flight to about 120 knots, hover, rearward and sideward flight to about 20 knots, auto rotations, and large-angle maneuvers Although the model is adequate for guidance and navigation studies at airspeeds greater than 120 knots, its handling characteristics fidelity is degraded due to the increasing effects of compressibility and the reverse flow region.

The following discussion applies to both the main and tail rotors, except where noted. Specific application to either the main or tail rotor is indicated by the subscripts m or t respectively.

Airspeed of rotor hub in control axes- The total airspeed of the rotor hub, in control axes, is required for calculation of the rotor forces and moments. This airspeed is initially determined in shaft axes, using the helicopter airspeed and angular velocity, and then transformed to control axes

$$\begin{bmatrix} u \\ v \\ w \end{bmatrix}_s = C_{s/h} \left(\begin{bmatrix} u \\ v \\ w \end{bmatrix}_{as,\ h} + \begin{bmatrix} 0 & z & -y \\ -z & 0 & x \\ y & -x & 0 \end{bmatrix}_{r,\ h} \begin{bmatrix} p \\ q \\ r \end{bmatrix}_h \right) \tag{13}$$

where

$$C_{s/h} = \begin{bmatrix} \cos \theta_s & 0 & -\sin \theta_s \\ \sin \theta_s \sin \phi_s & \cos \phi_s & \cos \theta_s \sin \phi_s \\ \sin \theta_s \cos \phi_s & -\sin \phi_s & \cos \theta_s \cos \phi_s \end{bmatrix} \tag{14}$$

and

$$\begin{bmatrix} u \\ v \\ w \end{bmatrix}_{as,\ h}$$

is defined by equation (1). The airspeed at the hub is transferred into control axes using the rotor orientation angle

$$\beta = \tan^{-1}\left(\frac{v_s + A_1' w_s}{u_s + B_1' w_s} \right)$$

which is obtained using the definition of control axes, that is

$$V_c \equiv 0$$

and using small angle approximations for the main rotor cyclic control inputs (swashplate angles), A_1' and B_1' (see fig. 2(c)),

$$\begin{bmatrix} u \\ v \\ w \end{bmatrix}_c = C_{c/s} \begin{bmatrix} u \\ v \\ w \end{bmatrix}_s \tag{15}$$

where

$$C_{c/s} = \begin{bmatrix} \cos \beta & \sin \beta & B_1' \cos \beta + A_1' \sin \beta \\ -\sin \beta & \cos \beta & A_1' \cos \beta - B_1' \sin \beta \\ -B_1' & -A_1' & 1 \end{bmatrix} \tag{16}$$

Note that the tail rotor does not have cyclic controls, and therefore the corresponding A_1' and B_1' are zero.

Rotor tip speed and induced flow ratios- The rotor forces and moments are functions of the rotor tip speed and induced inflow ratios, which are defined in terms of the hub airspeed in control axes, as

$$\mu = \frac{u_c}{\Omega R} \tag{17}$$

and

$$\lambda = \frac{w_c}{\Omega R} - \nu \tag{18}$$

respectively. The induced inflow ratio ν is obtained by filtering the steady-state value of ν. The resulting differential equation is

$$\dot{\nu} = \frac{1}{\tau_\nu}\left(\frac{C_T}{2\sqrt{\mu^2 + \lambda^2}} - \nu\right) \tag{19}$$

The time constant τ_ν is included to account for the lag associated with changes in rotor inflow. Note that the thrust coefficient C_T, defined below, and inflow ratio λ are functions of ν so that equation (19) is a first-order nonlinear differential equation.

Rotor thrust and coning angle in control axes- The rotor thrust, in control axes, and the coning angle a_o are calculated to the third power of the tip-speed ratio according to the following relations obtained from references 1 and 4:

$$T = bcR\rho(R\Omega)^2\left(\frac{C_T}{\sigma}\right) \tag{20}$$

and

$$a_o = \gamma\left[\left(\frac{1}{6}B^3 + 0.04\,\mu^3\right)\lambda + \left(\frac{1}{8}B^4 + \frac{1}{8}B^2\mu^2\right)\theta_o + \left(\frac{1}{10}B^5 + \frac{1}{12}B^3\mu^2\right)\theta_1\right] \tag{21}$$

where

$$\frac{C_T}{\sigma} = \frac{a}{2}\left[\left(\frac{1}{2}B^2 + \frac{1}{4}\mu^2\right)\lambda + \left(\frac{1}{3}B^3 + \frac{1}{2}B\mu^2 - \frac{4}{9\pi}\mu^3\right)\theta_o + \left(\frac{1}{4}B^4 + \frac{1}{4}B^2\mu^2\right)\theta_1\right] \tag{22}$$

and θ_o is the effective blade pitch angle at the root (collective pitch angle), and θ_1 is the blade twist. Note that a term involving the blade mass moment in equation (22) of reference 4 has been neglected in equation (21) above, for it contributes less than 0.5° and is essentially constant (ref. 1).

Rotor flapping angles in control axes- The calculation of the rotor flapping angles requires the fuselage angular velocity expressed in control axes:

$$\begin{bmatrix} p \\ q \\ r \end{bmatrix}_c = C_{c/s} C_{s/h} \begin{bmatrix} p \\ q \\ r \end{bmatrix}_h \tag{23}$$

where the transformation matrices are defined by equations (14) and (16).

The flapping angles a_1 and b_1 (fig. 2(d)) are calculated in control axes according to formulas obtained from reference 1.

$$a_1 = \frac{1}{[1 - (\mu^2/2B^2)]} \left[\left(2\lambda + \frac{8}{3}\theta_{0.75} \right)\mu + \frac{P_c}{\Omega} - \frac{16q_c}{B^4\gamma\Omega} \right] \tag{24}$$

and

$$b_1 = \frac{1}{[1 + (\mu^2/2B^2)]} \left[\frac{4}{3}\mu a_0 - \frac{q_c}{\Omega} - \frac{16p_c}{B^4\gamma\Omega} \right] \tag{25}$$

For a blade with linear twist and constant chord, it can be shown that replacing the θ_0 appearing in the references with the pitch at 3/4 radius $\theta_{0.75}$, and dropping θ_1 will have a negligible effect on the overall solution (ref. 1). The pitch at 3/4 radius is

$$\theta_{0.75} = \theta_0 + 0.75\ \theta_1 \tag{26}$$

Rotor drag force in control axes- The downwind component of the rotor force, in control axes, is

$$H = Ta' \tag{27}$$

where the small angle a' is a function of the useful and induced rotor drag-lift power and inflow (ref. 1), but behaves similarly to the longitudinal flapping angle a_1. An expression for a', which includes the effects of fuselage angular velocity (ref. 1), is

$$a' = \frac{1}{[1 - (\mu^2/2B^2)]} \left[\left(2\lambda + \frac{8}{3}\theta_{0.75} \right)\mu - \frac{24q_c}{B^4\gamma\Omega} \left(1 - \frac{0.29\ \theta_{0.75}}{C_T/\sigma} \right) \right] \tag{28}$$

Rotor side force in control axes- The rotor side force, in control axes is

$$J = bcR\rho(R\Omega)^2 \left(\frac{C_y}{\sigma} \right) \tag{29}$$

where

$$\frac{C_y}{\sigma} = \frac{a}{2}\left[\frac{3}{4} b_1 \lambda - \frac{3}{2} a_0 \mu\lambda + \frac{1}{4} a_1 b_1 \mu - a_0 a_1 \mu^2 + \frac{1}{6} a_0 a_1 - \left(\frac{3}{4} \mu a_0 - \frac{1}{3} b_1 - \frac{1}{2} \mu^2 b_1\right)\theta_{0.75}\right] \tag{30}$$

This equation, derived from equation (3) in reference 3, neglects angular velocity terms and uses the previous assumption involving the pitch at 3/4 radius, $\theta_{0.75}$.

Transformation of rotor forces to body axes- The rotor forces in control axes, given by equations (20), (27), and (29), are transformed to body axes,

$$\begin{bmatrix} X \\ Y \\ Z \end{bmatrix}_{r,\ h} = C^T_{s/h} C^T_{c/s} \begin{bmatrix} -H \\ J \\ -T \end{bmatrix}_c \tag{31}$$

where the transformation matrices are defined by equations (14) and (16).

Rotor torque in shaft axes- The rotor aerodynamic torque equation (ref.1), which accounts for both acceleration and deceleration, is

$$Q_a = bcR^2\rho(R\Omega)^2\left(\frac{C_Q}{\sigma}\right) \tag{32}$$

where

$$\frac{C_Q}{\sigma} = 0.00109 - 0.0036\lambda - 0.0027\theta_{0.75} - 1.10\lambda^2 - 0.545\lambda\theta_{0.75} + 0.122\theta^2_{0.75} + (0.00109 - 0.0027\theta_{0.75} - 3.13\lambda^2 - 6.35\lambda\theta_{0.75} - 1.93\theta^2_{0.75})\mu^2 - 0.133\lambda\theta_{0.75}\mu^3 + (-0.976\lambda^2 - 6.38\lambda\theta_{0.75} - 5.26\theta^2_{0.75})\mu^4 \tag{33}$$

The aerodynamic torque acting on the main rotor Q_{am}, is calculated using main rotor parameters in (32) and (33). The torque applied to the fuselage by the main rotor is a function of Q_{am} and is determined by the engine and governor model:

$$N_{hub,\ s} = Q_s \tag{34}$$

For the main rotor, Q_s is equal to the engine torque Q_{eng}. The tail rotor torque Q_{at}, calculated using tail rotor parameters in (32) and (33), is assumed to act directly on the fuselage so that Q_s is equal to Q_{at}.

Rotor hub moments in shaft axes- The hub moments due to flapping angle offsets are calculated in shaft axes according to formulas obtained from reference 1. These formulas result from neglecting higher order terms in equations presented in reference 3:

$$\begin{bmatrix} L \\ M \end{bmatrix}_{hub,\ s} = \frac{1}{2} eb\Omega^2 M_w \begin{bmatrix} b_1 \\ a_1 \end{bmatrix}_s \tag{35}$$

where

$$\begin{bmatrix} b_1 \\ a_1 \\ -- \end{bmatrix}_s = \begin{bmatrix} A_1' \\ -B_1' \\ 0 \end{bmatrix} + C^T_{c/s} \begin{bmatrix} b_1 \\ a_1 \\ 0 \end{bmatrix} \tag{36}$$

are the flapping angles in shaft axes.

Transformation of rotor moments to body axes- The rotor moments in shaft axes, given by equations (34) and (35), are transformed to body axes:

$$\begin{bmatrix} L \\ M \\ N \end{bmatrix}_{hub,\ h} = C^T_{s/h} \begin{bmatrix} L \\ M \\ N \end{bmatrix}_{hub,\ s} \tag{37}$$

The total moments applied to the fuselage by the rotor include the hub moments (37) and additional moments due to the location of the hub relative to the helicopter c.g.:

$$\begin{bmatrix} L \\ M \\ N \end{bmatrix}_{r,\ h} = \begin{bmatrix} L \\ M \\ N \end{bmatrix}_{hub,\ h} + \begin{bmatrix} 0 & -z & y \\ z & 0 & -x \\ -y & x & 0 \end{bmatrix}_{r,\ h} \begin{bmatrix} X \\ Y \\ Z \end{bmatrix}_{r,\ h} \tag{38}$$

where the rotor forces are defined by equation (31).

Tail rotor δ_3 hinge effect- The above model represents a rotor without a delta-three (δ_3) hinge, such as the main rotor of a CH-53. However, the tail rotor has a δ_3 hinge, so that blade coning and flapping affect blade pitch; therefore, the model is modified accordingly. Assuming the changes in blade pitch due to flapping are small compared with those due to coning,

$$\theta_{ot} = \theta_{ct} - a_{ot} \tan \delta_{3t} \tag{39}$$

where θ_{ct} is the value of collective pitch commanded by the control system. Note that the coning angle a_0, equation (21), is a function of θ_0; as a result, equations (21) and (39), for the tail rotor, should be solved simultaneously.

The inputs and outputs of the rotor models are shown in figures 3(c) and 3(d).

Engine and Governor Model

An engine and governor model is included to provide a realistic time delay between aerodynamic rotor torque and the resulting reaction torque applied to the fuselage. This model was adapted from one used by Boeing Vertol (ref. 1); although it is not a model of a CH-53 engine, it does provide the desired effects.

This model, which includes the effects of a gas turbine, a power turbine, rotor inertia, and shaft compliance, uses the reference rotor speed Ω_0 and the main rotor aerodynamic torque Q_{am} (eq. (32)) to calculate the angular velocities of the main and tail rotors and the engine torque. Note that the engine torque Q_{eng} is equal to the main rotor shaft torque Q_S in equation (34).

$$\left.\begin{aligned}
\dot{\Omega}_m &= [Q_{eng} - Q_{am} + K_d(\Omega_{pt} - \Omega_m)]/I_{mr} \\
\dot{Q}_{eng} &= K_c(\Omega_{pt} - \Omega_m) \\
\dot{\Omega}_{pt} &= [Q_{gen} + K_{gov}(\Omega_0 - \Omega_{pt}) - Q_{eng} - K_d(\Omega_{pt} - \Omega_m)]/I_{pt} \\
\dot{Q}_{gen} &= [Q_{am} - Q_{gen} + K_{gov}(\Omega_0 - \Omega_{pt})]/\tau_{eng} \\
\Omega_t &= 4.3\,\Omega_m
\end{aligned}\right\} \tag{40}$$

The constants K_c and K_d represent the main rotor shaft compliance and damping, respectively; note that the latter is required for computational stability. The Q_{am} term in the Q_{gen} differential equation allows the model to hold reasonably constant rotor speed under widely varying aerodynamic torques (ref. 1).

The inputs and outputs of the engine model are shown in figure 3(e).

Control System

The control system model, which includes the effects of pilot inputs, control cross coupling, an automatic flight control system (AFCS), and servo actuators, defines the main rotor collective pitch θ_{0m}, longitudinal and lateral cyclic pitch B_1 and A_1, and tail rotor collective pitch command θ_{ct}. This model was obtained from an unpublished Sikorsky Aircraft report.

Pilot controls-

$$\left.\begin{aligned} \theta_{om} &= K_1 + K_2 X'_{col} + \theta_{mafcs} \\ B_1 &= K_3 + K_4 X_{lon} + B_{1afcs} \\ A_1 &= K_5 + K_6 X'_{lat} + K_7 X'_{col} + A_{1afcs} \\ \theta_{ct} &= (K_8 + K_9 X_{ped} + K_{10} X'_{col}) + \theta_{tafcs} \end{aligned}\right\} \quad (41)$$

where

$$\left.\begin{aligned} X'_{col} &= X_{col} - 2.54 \text{ cm} \\ \text{or equivalently} & \\ X'_{col} &= X_{col} - 1.0 \text{ in.} \end{aligned}\right\} \text{ if } X_{col} > 2.54 \text{ cm or } X_{col} > 1.0 \text{ in.}$$

$$X'_{col} = 0 \quad \text{if} \quad X_{col} \leq 2.54 \text{ cm} \quad \text{or} \quad X_{col} \leq 1.0 \text{ in.}$$

and the term in parentheses is limited to the range of -0.0349 rad (-2.0°) to +0.419 rad (+24.0°).

The pilot inputs, in equation (41), are the displacements of the pilot controls relative to a nominal position. These positions are shown in the control rigging diagrams, figures 13(a)-13(d), as the zero displacement positions. The force characteristics of the pilot controls are given in table 2.

AFCS inputs- The following features of the AFCS are not implemented, directly, due to hardware limitations of the fixed-base simulator used in conjunction with this model:

1. Trim adjustments for various c.g. locations

2. Indicator of AFCS authority used

3. Supplemental controller which changes effective collective stick position

4. "Open-loop" pedal spring

5. Lateral cyclic "stick pusher"

Effects of these features that are considered critical to the anticipated flying tasks are included by modifying the AFCS model obtained from Sikorsky Aircraft.

The absence of trim adjustments is compensated for by placing the c.g. at fuselage station 332 so that the mathematical model trims straight and level at 90 knots, with minimal AFCS contribution to the longitudinal cyclic pitch; that is $B_{1afcs} \approx 0$. Problems caused by the lack of information on AFCS authority used are alleviated by (1) increasing the limits on the AFCS contribution to the tail rotor pitch command θ_{tafcs} (table 5); (2) removing θ_{tafcs} from the bracketed term in equation (41), which is limited; and (3) selection of the c.g. fuselage station discussed above. The effects of the collective stick supplemental controller are not considered critical and, therefore, are not included. The "open-loop" pedal spring is represented by the integral term $K_{\lambda 3}/s$ in the θ_{tafcs} equation (42). The basic effects of the lateral cyclic "stick pusher" are to provide the pilot with a stick force proportional to the deviation of roll attitude from its trim value, and to return the vehicle to its trim roll attitude when the pilot releases the stick. Since a "control loader" is not available in the fixed-base simulator, implementation of these effects required several changes to the AFCS model; the changes are described in detail below.

In the original AFCS the roll trim reference is removed from the lateral channel, A_{1afcs} in equation (42), when the pilot places his feet on the pedals (activating a pressure sensitive switch) prior to a lateral maneuver. If the pilot releases lateral stick pressure during the maneuver and keeps his feet on the pedals, the "stick pusher" moves the stick so as to regain the roll trim reference attitude. This characteristic is obtained by removing the roll trim reference from A_{1afcs} in equation (42) only when the lateral stick is displaced 1.27 cm (0.5 in.) or more from its zero force trim position. Thus, the roll reference is removed when the pilot, by displacing the stick laterally, indicates a desire to maneuver; the reference is regained when the pilot releases his control force, allowing the stick to return to its zero force position. The control forces provided by the "stick pusher" during the maneuver are obtained by adding a bias proportional to the roll deviation from trim to the lateral stick displacement (see X'_{lat}, eq. (42)). This causes the steady-state roll attitude deviation from trim to be proportional to lateral stick displacement from the zero force trim position and, therefore, proportional to the control force required by the pilot. The bias gain, $K_{\lambda 4}$, in equation (42) corresponds to 0.14 N (0.08 lb) of pilot force per degree change in roll attitude.

The control inputs from the modified AFCS model which contains altitude hold, heading hold, and turn coordination modes, are

$$\theta_{mafcs} = \underbrace{I_{ah}K_{11}(h_c - h)}_{\text{altitude hold}}$$

$$B_{1afcs} = \left[\begin{matrix}\text{fade in/out}\\ \text{circuit no. 1}\end{matrix}\right]\left[\left(K_{12} + \frac{K_{13}s}{(\tau_1 s + 1)^2}\right)\theta_h + \frac{K_{14}}{\tau_2 s + 1}X_{\ell on}\right]$$

$$A_{1afcs} = \left[\begin{matrix}\text{fade in/out}\\ \text{circuit no. 2}\end{matrix}\right]\left[\frac{K_{15}}{\tau_3 s + 1}p_h + \underbrace{\left(\begin{matrix}\text{fade in/out}\\ \text{circuit no. 3}\end{matrix}\right)K_{16}I_{trim}(\phi_{trim} - \phi)_h}_{\text{heading hold}}\right]$$

$$+ \underbrace{I_{ah}K_{17}(h_c - h)}_{\text{altitude hold}}$$

$$\theta_{tafcs} = \left(1 + \frac{K_{23}}{s}\right)\left[\left(\begin{matrix}\text{fade in/out}\\ \text{circuit no. 4}\end{matrix}\right)\left[\underbrace{K_{18}I_{tc}p_h}_{\text{turn coordination}} + \frac{K_{19}s}{\tau_4 s + 1}r_h + \underbrace{I_{ped}K_{20}(\phi_{trim} - \phi)_h}_{\text{heading hold}}\right] + \underbrace{I_{tc}K_{21}a_y}_{\text{turn coordination}}\right] + \underbrace{I_{ah}K_{22}(h_c - h)}_{\text{altitude hold}}$$

$$X'_{\ell at} = X_{\ell at} + \left[1 - \left(\begin{matrix}\text{fade in/out}\\ \text{circuit no. 3}\end{matrix}\right)\right]K_{24}I_{trim}(\phi_{trim} - \phi)_h \qquad (42)$$

The fade in/out circuits are intended to minimize the introduction of large transients to the flight control system due to changes in the AFCS operating mode. The gain of these circuits varies between zero and unity, according to the transfer functions listed in table 3. It should be noted that these transfer functions are only used to determine gain values, and do not represent actual filters.

AFCS modes- The operational modes of the AFCS are controlled by the following variables, which appear in equation (42).

I_{ah} = 1 Altitude hold mode engaged
= 0 Altitude hold mode disengaged

I_{afcs} = 1 AFCS engaged
= 0 AFCS disengaged

I_{ped} = 1 Pilot's feet off pedals
= 0 Pilot's feet on pedals

I_{trim} = 1 Cyclic trim button released
= 0 Cyclic trim button depressed

$I_{tc} = 1$ Above 60 knots and pilot's feet on pedals
$= 0$ At or below 60 knots or pilot's feet off pedals

$I_{X\ell at} = 1$ Lateral stick within 0.5 in. of zero force trim position
$= 0$ Lateral stick beyond 0.5 in. of zero force trim position

The values of the roll and heading trim angles, ϕ_{trim} and ψ_{trim} respectively, are determined as follows: ϕ_{trim} is set equal to the current ϕ_h when the cyclic trim button is released; ψ_{trim} is set equal to the current ψ_h when the pilots feet move off the pedals.

The AFCS and the altitude-hold mode are activated by switches on the instrument panel. The heading-hold and turn-coordination modes are controlled by airspeed and location of the pilot's feet (either on or off the pedals). The heading-hold mode is engaged whenever the pilot's feet are off the pedals, regardless of airspeed. The turn-coordination mode is engaged only when the pilot's feet are on the pedals and the airspeed is greater than 60 knots. The operation of these modes is summarized in table 4.

AFCS authority limits- The authority of the AFCS is limited so that it can be overridden by the pilot. This is accomplished by limiting the control inputs from the AFCS, equation (42), to the values shown in table 5. In the expressions for A_{1afcs} and θ_{tafcs} the limits are imposed prior to the addition of the altitude-hold terms.

Servo actuators- The primary servo actuators transform the main rotor control commands, given in equation (41), into swashplate angles and blade collective pitch. The following model of these servos was obtained from Sikorsky Aircraft.

$$\begin{bmatrix} \theta'_{om} \\ B'_1 \\ A'_1 \end{bmatrix}_{(s)} = \frac{\omega_n^2 e^{-t_o s}}{(s^2 + 2\zeta\omega_n s + \omega_n^2)(\tau s + 1)} \begin{bmatrix} \theta_{om} \\ B_1 \\ A_1 \end{bmatrix}_{(s)} \tag{43}$$

A model of the tail rotor servo was not obtained from Sikorsky; therefore, it was assumed that

$$\theta'_{ct} = \theta_{ct} \tag{44}$$

Approximations for real-time simulation- During use of this helicopter model in real-time guidance and navigation studies it may be desirable to neglect some of the relatively high-frequency dynamics — specifically, the relatively small time constants, τ_1 and τ_3, in equation (42), and the servo dynamics, equation (43).

The inputs and outputs of the control system model are shown in figure 3(f).

Equations of Motion

The helicopter equations of motion are given in body axes with respect to a flat, nonrotating Earth. The helicopter is considered a rigid body with mass symmetry about the $x_h - z_h$ plane. The effects due to the engine angular momentum are neglected.

Translational acceleration- The translational equations of motion are

$$C_{h/e}\begin{bmatrix}0\\0\\mg\end{bmatrix} + \begin{bmatrix}X\\Y\\Z\end{bmatrix}_{f,\,h} + \begin{bmatrix}X\\Y\\Z\end{bmatrix}_{r,\,h} = m\left(\begin{bmatrix}\dot{u}\\\dot{v}\\\dot{w}\end{bmatrix}_{cg,\,h} + \begin{bmatrix}0 & -r & q\\ r & 0 & -p\\ -q & p & 0\end{bmatrix}_h \begin{bmatrix}u\\v\\w\end{bmatrix}_{cg,\,h}\right) \tag{45}$$

where

$$C_{h/e} = \begin{bmatrix} \cos\theta\cos\psi & \cos\theta\sin\psi & -\sin\theta \\ \sin\phi\sin\theta\cos\psi - \cos\phi\sin\psi & \cos\phi\cos\psi + \sin\phi\sin\theta\sin\psi & \sin\phi\cos\theta \\ \cos\phi\sin\theta\cos\psi + \sin\phi\sin\psi & \cos\phi\sin\theta\sin\psi - \sin\phi\cos\psi & \cos\phi\cos\theta \end{bmatrix}_h \tag{46}$$

and ϕ_h, θ_h, and ψ_h are the Euler angles that define the orientation of the body axis system (fig. 3). The fuselage aerodynamic forces are given by equation (10), and the rotor forces, which include those due to both main and tail rotors, are given by equation (31). Equation (45) can be rearranged to yield

$$\begin{bmatrix}\dot{u}\\\dot{v}\\\dot{w}\end{bmatrix}_{cg,\,h} = \frac{1}{m}\left(\begin{bmatrix}X\\Y\\Z\end{bmatrix}_{f,\,h} + \begin{bmatrix}X\\Y\\Z\end{bmatrix}_{r,\,h}\right) - \begin{bmatrix}0 & -r & q\\ r & 0 & -p\\ -q & p & 0\end{bmatrix}_h \begin{bmatrix}u\\v\\w\end{bmatrix}_{cg,\,h} + C_{h/e}\begin{bmatrix}0\\0\\g\end{bmatrix} \tag{47}$$

Inertial velocity and position- The inertial velocity, in body coordinates, is obtained by integrating equation (47), with respect to time, subject to appropriate initial conditions. The inertial velocity in Earth axes is

$$\begin{bmatrix}u\\v\\w\end{bmatrix}_{cg,\,e} = C^T_{h/e}\begin{bmatrix}u\\v\\w\end{bmatrix}_{cg,\,h} \tag{48}$$

The position of the helicopter, in Earth coordinates, is determined by integrating equation (48) with the appropriate initial conditions.

$$\begin{bmatrix}\dot{x}\\ \dot{y}\\ \dot{z}\end{bmatrix}_{cg,\ e} = \begin{bmatrix}u\\ v\\ w\end{bmatrix}_{cg,\ e} \tag{49}$$

Angular acceleration- The rotational equations of motion are

$$\begin{bmatrix}L\\ M\\ N\end{bmatrix}_{f,\ h} + \begin{bmatrix}L\\ M\\ N\end{bmatrix}_{r,\ h} = I_h\begin{bmatrix}\dot{p}\\ \dot{q}\\ \dot{r}\end{bmatrix}_h + \begin{bmatrix}0 & -r & q\\ r & 0 & -p\\ -q & p & 0\end{bmatrix}_h I_h\begin{bmatrix}p\\ q\\ r\end{bmatrix}_h \tag{50}$$

where

$$I_h = \begin{bmatrix}I_{xx} & 0 & I_{xz}\\ 0 & I_{yy} & 0\\ I_{xz} & 0 & I_{zz}\end{bmatrix}$$

The fuselage aerodynamic moments are given by equation (11), and the rotor moments, which include those due to both the main and tail rotors, are given by equation (38). Equation (50) can be rearranged to yield

$$\begin{bmatrix}\dot{p}\\ \dot{q}\\ \dot{r}\end{bmatrix}_h = I_h^{-1}\left[\begin{bmatrix}L\\ M\\ N\end{bmatrix}_{f,\ h} + \begin{bmatrix}L\\ M\\ N\end{bmatrix}_{r,\ h} - \begin{bmatrix}0 & -r & q\\ r & 0 & -p\\ -q & p & 0\end{bmatrix} I_h\begin{bmatrix}p\\ q\\ r\end{bmatrix}_h\right] \tag{51}$$

Angular velocity and orientation- The angular velocity, in body axes, is obtained by integrating equation (51), with respect to time, subject to the appropriate initial conditions.

The helicopter Euler angles are determined by integrating

$$\begin{bmatrix}\dot{\phi}\\ \dot{\theta}\\ \dot{\psi}\end{bmatrix} = C^{-1}\begin{bmatrix}p\\ q\\ r\end{bmatrix} \tag{52}$$

where

$$C = \begin{bmatrix}1 & 0 & -\sin\theta\\ 0 & \cos\phi & \sin\phi\cos\theta\\ 0 & -\sin\phi & \cos\phi\cos\theta\end{bmatrix}_h \tag{53}$$

The inputs and outputs of the equations of motion are shown in figure 3(g).

MODEL VALIDATION

The mathematical model is validated by comparing its response to that of an actual helicopter and by a qualitative comparison of the handling characteristics made by experienced pilots.

Time History Comparisons

The most readily available flight data were from an HH-53C, an Air Force version of a CH-53C, which has two external fuel tanks. Since the HH-53C response time histories given in reference 6 were obtained with these tanks full, the helicopter inertias in the model were modified accordingly in order to provide a more realistic comparison of responses. The following modified parameters were calculated using data supplied by Sikorsky Aircraft.

$$\left.\begin{aligned} I_{xx,h} &= 56{,}367 \text{ kg-m}^2 \\ &= 41{,}553 \text{ slug-ft}^2 \\ I_{yy,h} &= 268{,}709 \text{ kg-m}^2 \\ &= 198{,}090 \text{ slug-ft}^2 \\ I_{zz,h} &= 248{,}745 \text{ kg-m}^2 \\ &= 183{,}373 \text{ slug-ft}^2 \\ I_{xz,h} &= 28{,}400 \text{ kg-m}^2 \\ &= 20{,}936 \text{ slug-ft}^2 \end{aligned}\right\} \tag{54}$$

The aerodynamics effects of the external tanks were not known and, therefore, not incorporated into the model. Reference 6 contained HH-53C time histories for pulse type inputs to the longitudinal cyclic, lateral cyclic, and pedals, at the following flight condition with the AFCS both on and off.

$$\left.\begin{aligned} \text{Air speed} &= 113 \text{ knots} \\ \text{Altitude} &= 7000 \text{ ft} \\ \text{Main rotor speed} &= 185 \text{ rpm} \\ \text{Gross weight} &= 41{,}000 \text{ lb} \\ \text{FSCG} &= 328 \\ \text{Atmospheric temperature} &= -18^\circ \text{ C} \end{aligned}\right\} \tag{55}$$

The response time history of the CH-53 model at the above flight condition was obtained using a "dynamic check" routine. This routine provided the model with flight control inputs that approximated those of the HH-53C. Also, this routine was used to control the operational modes of the AFCS, as will be discussed later. The time histories of the CH-53 model and the HH-53C are compared with the AFCS on; this is done because the model will normally be operated in this mode for terminal-area studies.

A comparison of the responses to a forward longitudinal cyclic pulse, shown in figure 14(a), indicates good agreement for the Euler angles and for

the body-axis angular velocities. This is also the case for the responses to a right lateral cyclic pulse, shown in figure 14(b). Here it is assumed that the HH-53C response was obtained with the cyclic trim button depressed, since the roll attitude does not return to zero after the pulse. This condition was simulated in the model by using the dynamic check routine to set $I_{trim} = 0$ in equations (42). The responses to a right pedal pulse did not compare as well as those for the previous inputs. The model produced much larger attitude excursions than indicated for the HH-53C response. A reasonable comparison, shown in figure 14(c), was obtained by raising the damping gain K_{19} from 0.573 to 1.50.

Possible sources of the discrepancy are the unmodeled aerodynamics of the HH-53C external fuel tanks, and features of the AFCS which were modified or not included due to limitations of the fixed-base simulator. An attempt was made to compensate for differences between the actual and modeled AFCS by controlling the modes of the latter with the dynamic check routine. For the response to a pedal pulse, this routine simulated the AFCS transformation from the heading-hold mode to the turn-coordination mode by setting $I_{ped} = 0$ and $I_{trim} = 0$ in equations (42). Later review indicated that this is a poor method for simulating the mode transformation. The above method completely removes the roll trim reference when the pedal pulse is initiated. Actually, this reference should fade out with a 1-sec time constant and, therefore, a more realistic simulation would keep $I_{trim} = 1$ and set $I_{xlat} = 0$ and $I_{ped} = 0$ at the beginning of the pulse. It may also be desirable to eliminate effects of the "stick pusher" by setting $K_{24} = 0$ in equation (42). Because the method used in simulating the AFCS mode transformation served to prematurely remove an attitude error signal, it probably increased the attitude excursions of the model and, therefore, may have contributed to the response discrepancy.

Pilot Comments

A qualitative evaluation of the mathematical model was made by two pilots using a fixed-base simulator with visual scene. These evaluations were to be made considering the intended use of the model, that is, terminal-area guidance and navigation studies.

The control forces and general feel of the flight controls were satisfactory, although the absence of breakout and gradient forces, with the cyclic trim button depressed, results in stick-jump and a tendency to overcontrol. The absence of cyclic beeper trim and collective and pedal parallel servos did not degrade the model for its intended use. The basic AFCS functions were primarily evaluated in forward flight at approach speeds (90-120 KIAS). The retention of trimmed airspeed and pitch and roll attitude was excellent. The AFCS modes, altitude-hold, heading-hold, and turn-coordination operated satisfactorily. Also, the AFCS modifications, made to include effects of a lateral "stick pusher," provided responses that were much more characteristic of the aircraft. Although, not required, low-speed flight and hover were also evaluated. The attitude- and heading-hold features operated very well during decelerating approaches to a 50-ft hover. The collective increases and nose-high attitudes required during deceleration were similar to those of the [illegible]

aircraft. Above 10 knots, turns were easily coordinated with the pedals. At lower speeds, in forward and sideward flight and in hover, precise heading and hover control required much closer pilot attention to the turn coordinator. This was mainly due to insufficient motion cues from the visual scene.

It was concluded that the flying qualities of this model were qualitatively representative of the actual aircraft, within the limitation of a fixed-base simulator.

CONCLUSIONS

The mathematical model of a CH-53 helicopter described in this report was developed for real-time piloted simulation in support of terminal-area guidance and navigation studies. This model is based on modified nonlinear classical rotor theory and nonlinear fuselage aerodynamics. Limitations of the fixed-base simulation facility prevented direct implementation of several features of the automatic flight control system (AFCS). The effects of these features considered critical to the anticipated flying tasks were included by modifying the AFCS equations. The model was validated by comparing its response with actual flight data and by a qualitative comparison of the handling characteristics made by experienced pilots. These comparisons indicated that the model is satisfactory for terminal area guidance and navigation studies.

REFERENCES

1. Schannessy, J. D.; Deaux, Thomas N.; and Yenni, Kenneth R.: The Development and Validation of a Piloted Simulation of a Helicopter and External Sling Load. NASA TP-1285, 1979.

2. Wilcock, T.; and Thorpe, Ann C.: Flight Simulation of a Wessex Helicopter — A Validation Exercise. C.P. No. 1299, British A.R.C., 1974.

3. Seckel, Edward; and Curtiss, H. C., Jr.: Aerodynamic Characteristics of Helicopter Rotors. Report No. 659, Department of Aerospace and Mechanical Science, Princeton U., Princeton, N.J., Dec. 1963.

4. Bailey, F. J., Jr.: A Simplified Theoretical Method of Determining the Characteristics of a Lifting Rotor in Forward Flight. NACA Rep. 716, 1941.

5. Amer, Kenneth B.; and Gustafson, F. B.: Charts for Estimation of Longitudinal-Stability Derivatives for a Helicopter Rotor in Forward Flight. NACA TN-2309, 1951.

6. Barbini, Wayne J.; Balfe, P. J.; Lovrien, C. E., Jr.: Category II Performance and Flying Qualities Tests of the HH-53C Helicopter. AFFTC-TR-70-8, Air Force Flight Test Center, Edwards AFB, Calif., Feb. 1970.

TABLE 1.- VALUES OF PARAMETERS FOR CH-53 HELICOPTER
[Subscripts m and t denote main and tail rotor, respectively]

a_m, per rad	5.73	i_{to}, rad (deg)	0.0524 (3.0)
a_t, per rad	5.73	K_c, N-m/(rad/sec) [ft-lb/(rad/sec)]	1572000 [1159209]
BLCG, m (in.)	0.0 (0.0)	K_d, N-m/(rad/sec) [ft-lb/(rad/sec)]	132000 [97338]
B_m	0.97	K_f, m (ft)	0.099 (0.327)
B_t	0.97	K_{gov}, N-m/(rad/sec) [ft-lb/(rad/sec)]	.833.3 (614)
b_m	6	K_1, rad (deg)	0.0436 (2.5)
b_t	4	K_2, rad/cm (deg/in.)	0.00989 (1.44)
c_m, m (ft)	0.66 (2.165)	K_3, rad (deg)	0.0524 (3.0)
c_t, m (ft)	0.391 (1.284)	K_4, rad/cm (deg/in.)	0.0146 (2.13)
e_{kf}	0.5	K_5, rad (deg)	-0.0175 (-1.0)
e_{kt}	1.8	K_6, rad/cm (deg/in.)	0.00930 (1.35)
e_m, m (ft)	0.610 (2.0)	K_7, rad/cm (deg/in.)	-0.000989 (-0.144)
e_t, m (ft)	0.122 (0.4)	K_8, rad (deg)	0.0262 (1.5)
FSCG, m (in.)	8.433 (332.0)	K_9, rad/cm (deg/in.)	0.0364 (5.30)
G_{gov}, N-m/(rad/sec) [ft-lb/(rad/sec)]	85160 [62798]	K_{10}, rad/cm (deg/in.)	0.00989 (1.44)
I_{bm}, kg-m^2 (slug-ft^2)	5489 (4046)	K_{11}, rad/m (deg/ft)	0.000778 (0.0136)
I_{bt}, kg-m^2 (slug-ft^2)	22.72 (16.75)	K_{12}	0.60
I_{mr}, kg-m^2 (slug-ft^2)	40478 (29840)	K_{13}, sec	0.32
I_{pt}, kg-m^2 (slug-ft^2)	4325 (3188)	K_{14}, rad/cm (deg/in.)	0.00756 (1.10)
$I_{xx,h}$, kg-m^2 (slug-ft^2)	48891 (36041)	K_{15}, sec	-0.15
$I_{yy,h}$, kg-m^2 (slug-ft^2)	239491 (176551)	K_{16}	0.24
$I_{zz,h}$, kg-m^2 (slug-ft^2)	223361 (164660)	K_{17}, rad/m (deg/ft)	-0.0000778 (-0.00136)
$I_{xz,h}$, kg-m^2 (slug-ft^2)	22518 (16600)		

TABLE 1.- Continued

K_{18}, sec . . . . . -0.081	δ_{3m}, rad (deg) 0.0 (0.0)
K_{19}, sec^2 . . . . . 1.50	δ_{3t}, rad (deg) 0.78 (45)
K_{20} . . . . . -0.216	ζ 0.2
K_{21}, rad/m/sec^2 (deg/ft/sec^2) . . . 0.0162 (0.283)	θ_{sm}, rad (deg) . . . . . -0.0873 (-5.0)
K_{22}, rad/m (deg/ft) 0.000778 (0.0136)	θ_{st}, rad (deg) 0.0 (0.0)
K_{23}, sec^{-1} 0.830	θ_{1m}, rad (deg) . . . . . -0.105 (-6.0)
K_{24}, m/rad (m/deg) 0.143 (0.0025)	θ_{1t}, rad (deg) . . . . . -0.140 (-8)
M_{wm}, kg-m (slug-ft) 819 (184.1)	σ_m 0.1145
M_{wt}, kg-m (slug-ft) 18.76 (4.2)	σ_t 0.2042
m_h, kg (lb) 15,227 (33,500)	τ, sec 0.012
R_m, m (ft) 11.01 (36.11)	τ_{eng}, sec 0.50
R_t, m (ft) 2.44 (8.0)	τ_{vm}, sec 0.20
t_o, sec 0.02	τ_{vt}, sec 0.20
WLCG, m (in.) 4.149 (163.3)	τ_1, sec 0.013
$x_{r_m,h}$, m (ft) . . . . . -0.112 (-0.368)	τ_2, sec 1.4
$y_{r_m,h}$, m (ft) 0.0 (0.0)	τ_3, sec 0.016
$z_{r_m,h}$, m (ft) . . . . . -2.438 (-7.81)	τ_4, sec 1.8
$x_{r_t,h}$, m (ft) . . . . . -13.68 (-44.85)	τ_5, sec 4.0
$y_{r_t,h}$, m (ft) . . . . . -0.853 (-2.8)	τ_6, sec 1.0
$z_{r_t,h}$, m (ft) . . . . . -2.819 (-9.06)	τ_7, sec 1.0
$x_{wt,h}$, m (ft) . . . . . -0.102 (-0.333)	τ_8, sec 1.0
$y_{wt,h}$, m (ft) 0.0 (0.0)	ϕ_{sm}, rad (deg) 0.0 (0.0)
$z_{wt,h}$, m (ft) 0.0584 (0.16)	ϕ_{st}, rad (deg) 1.57 (90)
$x_{ps,h}$, m (ft) 4.827 (15.83)	ω_{om}, rad/sec 19.3
$y_{ps,h}$, m (ft) . . . . . --- (---)	ω_{ot}, rad/sec 82.9
$z_{ps,h}$, m (ft) . . . . . -0.2083 (-0.6833)	ω_m, rad/sec 95.0

TABLE 2.- FORCE CHARACTERISTICS OF PILOT CONTROLS

Pilot control	Force	
	Breakout, N (lb)	Gradient, N/cm (lb/in.)
Longitudinal cyclic	8.9 (2.0)	2.3 (1.3)
Lateral cyclic	6.7 (1.5)	1.4 (0.8)
Collective	20 (4.5)	0 (0)
Pedals	36 (8.0)	5.3 (3.0)

TABLE 3.- GAINS OF FADE IN/OUT

Circuit number			
1	2	3	4
$\frac{I_{afcs}}{\tau_5 s + 1}$	$\frac{I_{afcs}}{\tau_6 s + 1}$	$\frac{I_{x\ell at}}{\tau_7 s + 1}$	$\frac{I_{afcs}}{\tau_8 s + 1}$

TABLE 4.- SUMMARY OF HEADING-HOLD AND TURN-COORDINATION MODE LOGIC

Operating condition		Feedback information				Mode
Airspeed	Pilots feet	Roll pos.	Heading	Roll rate	Lat. acc.	
Above 60 knots	On pedals	Off	Off	On	On	Turn-coord.
	Off pedals	On	On	Off	Off	Head.-hold
Below 60 knots	On pedals	Off	Off	Off	Off	---
	Off pedals	On	On	Off	Off	Head.-hold

TABLE 5.- AUTHORITY LIMITS OF AFCS

AFCS input	Limits, rad (deg)
θ_{mafcs}	±0.0227 rad, (±1.3)
B_{1afcs}	±0.0454, (±2.6)
A_{1afcs}	±0.0209, (±1.2)
θ_{tafcs}	±0.0332, (±1.9)[a]

[a]This limit increased to ±7° in the simulation.

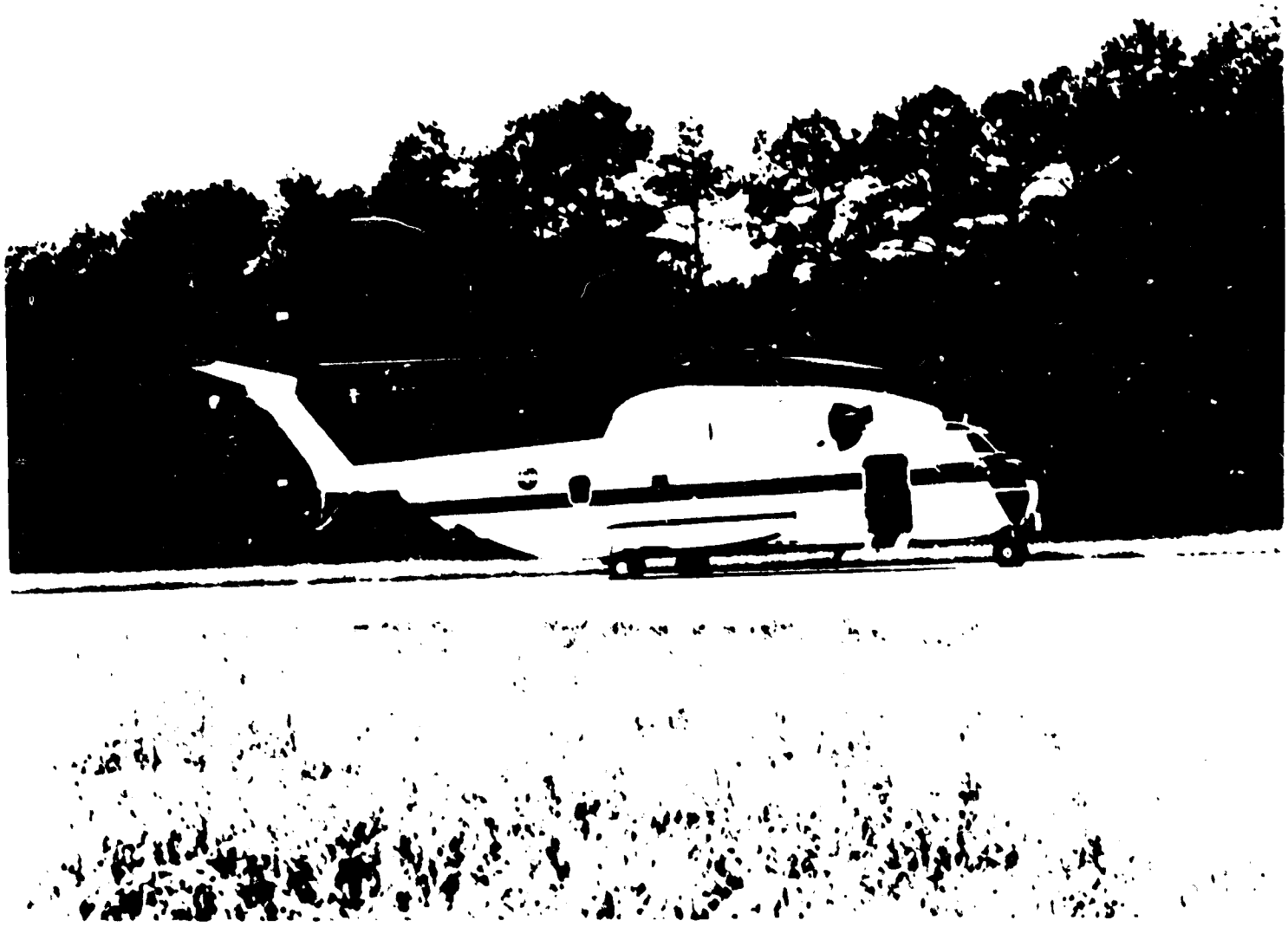

Figure 1.- Sikorsky CH-53.

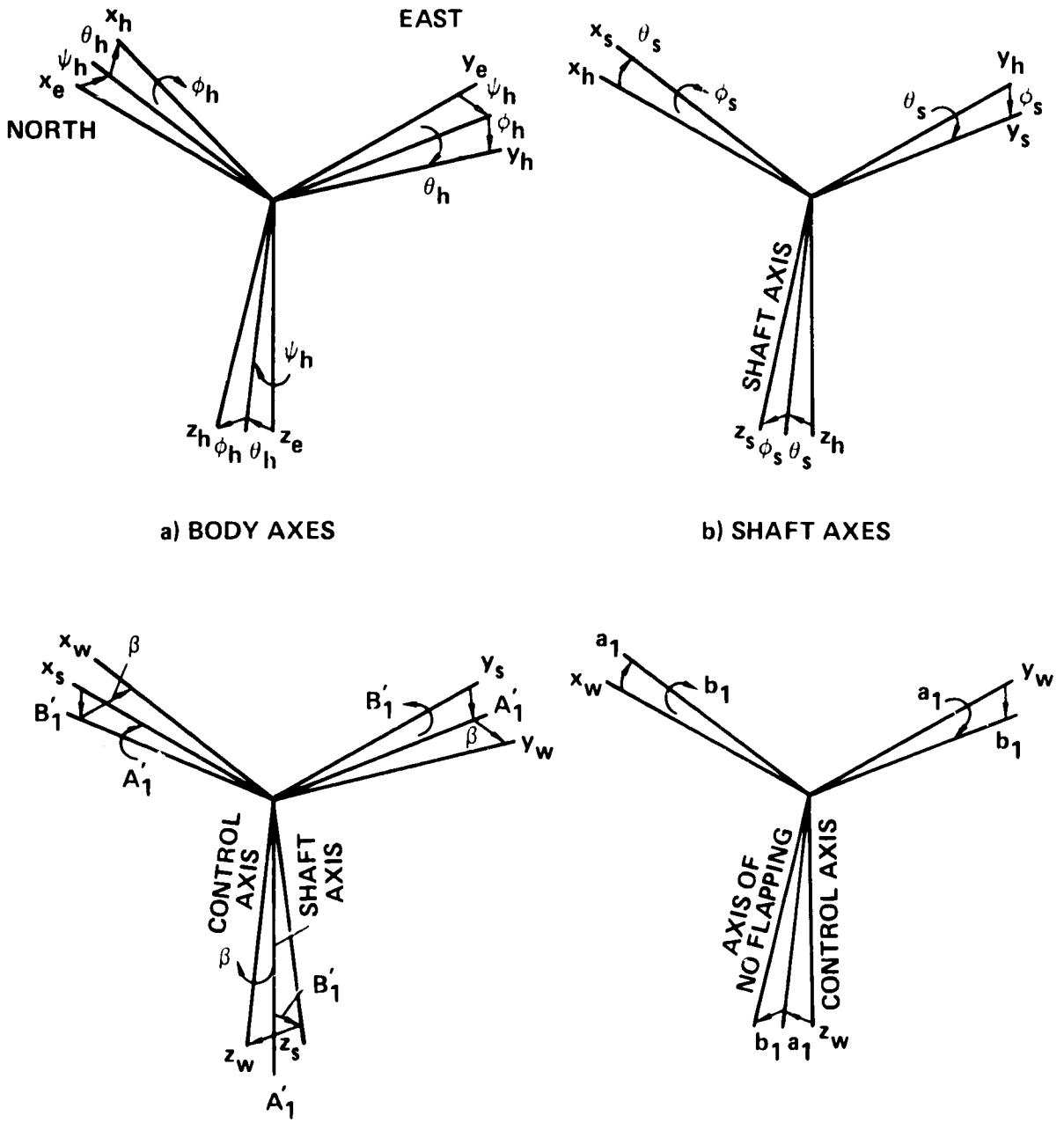

Figure 2.- Helicopter body axes, shaft axes, control axes, and flapping angle definitions.

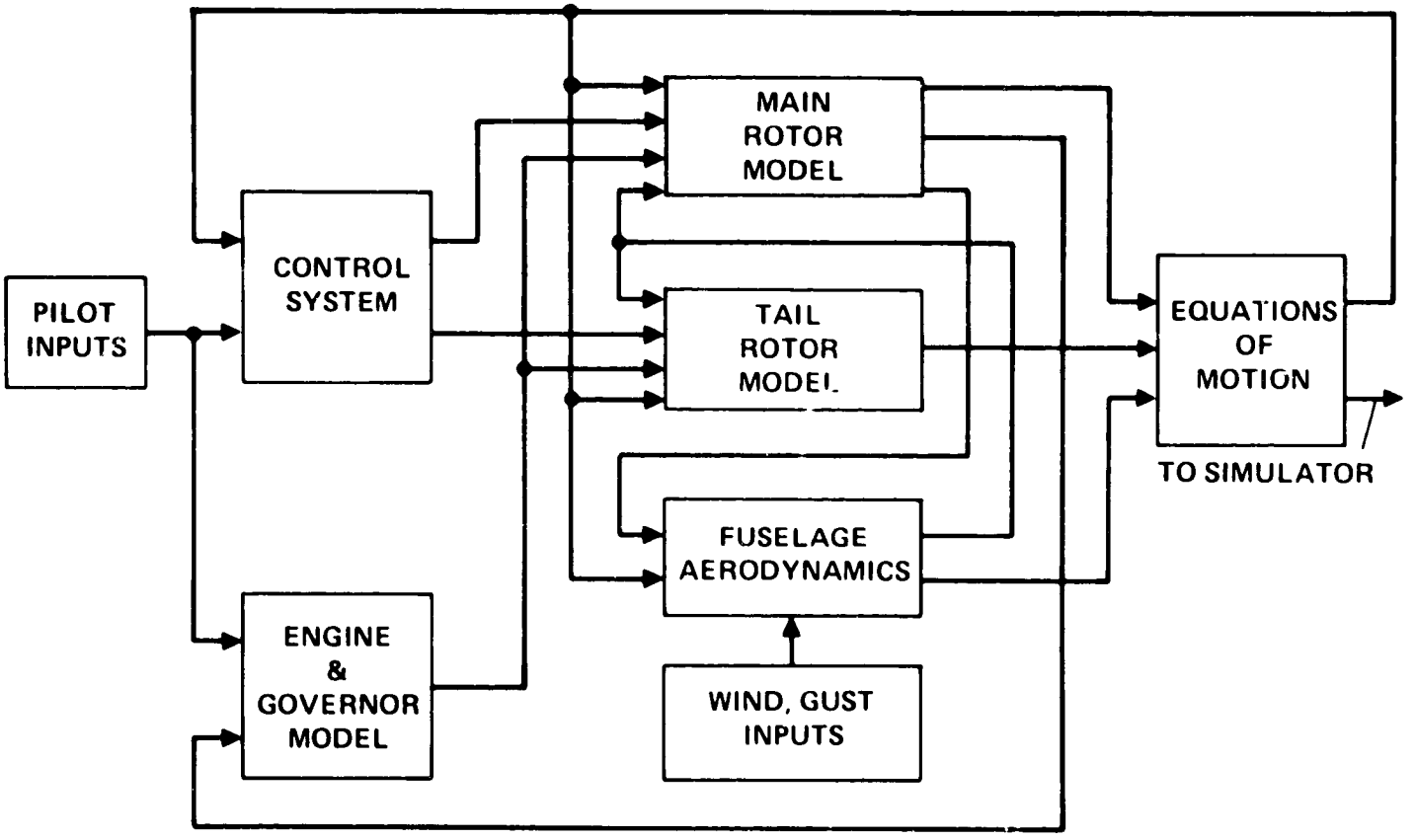

(a) Helicopter simulation.

Figure 3.- Block diagram of helicopter model and input-output diagrams of individual component models.

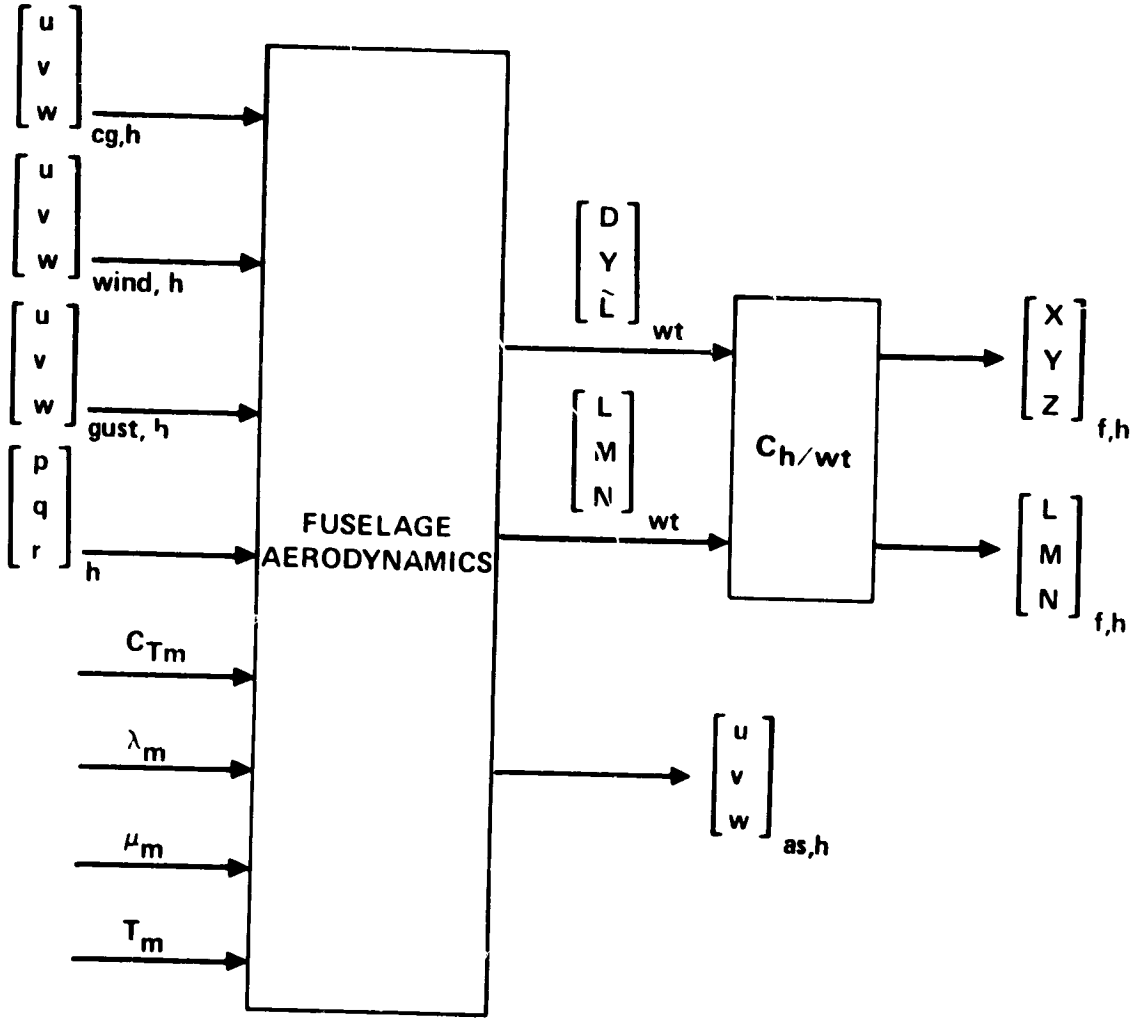

(b) Fuselage aerodynamics model.

Figure 3.- Continued.

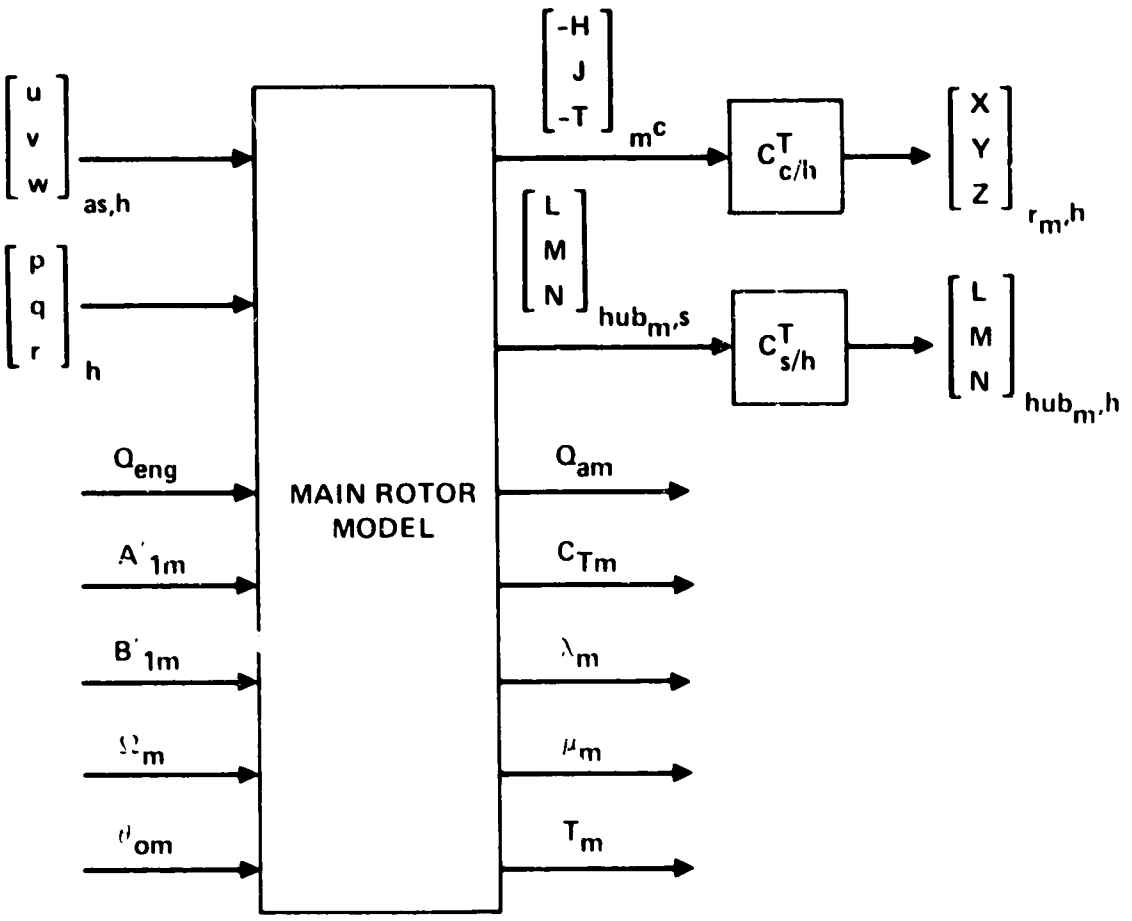

(c) Main rotor (subscript m) model.

Figure 3.- Continued.

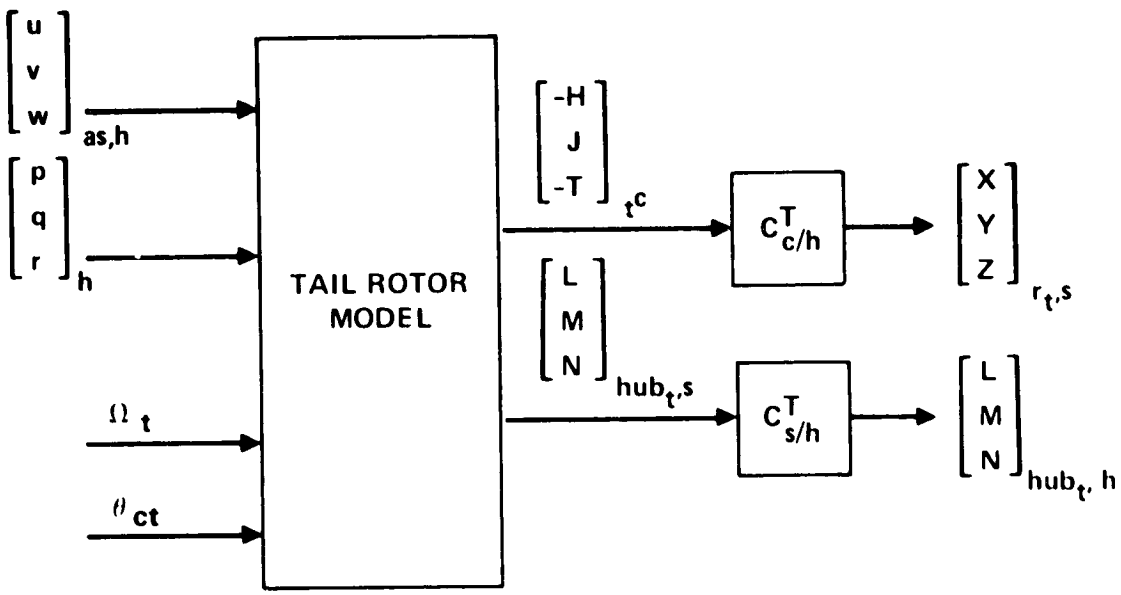

(d) Tail Rotor (subscript t) model.

Figure 3.- Continued.

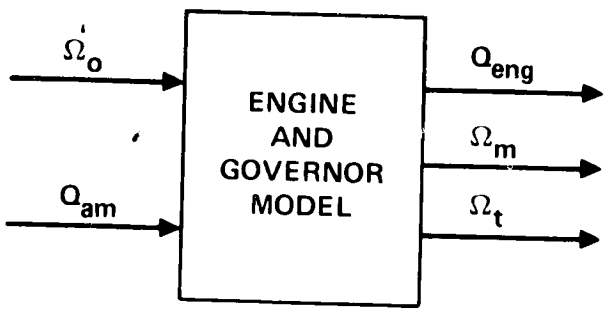

(e) Engine and governor model.

Figure 3.- Continued.

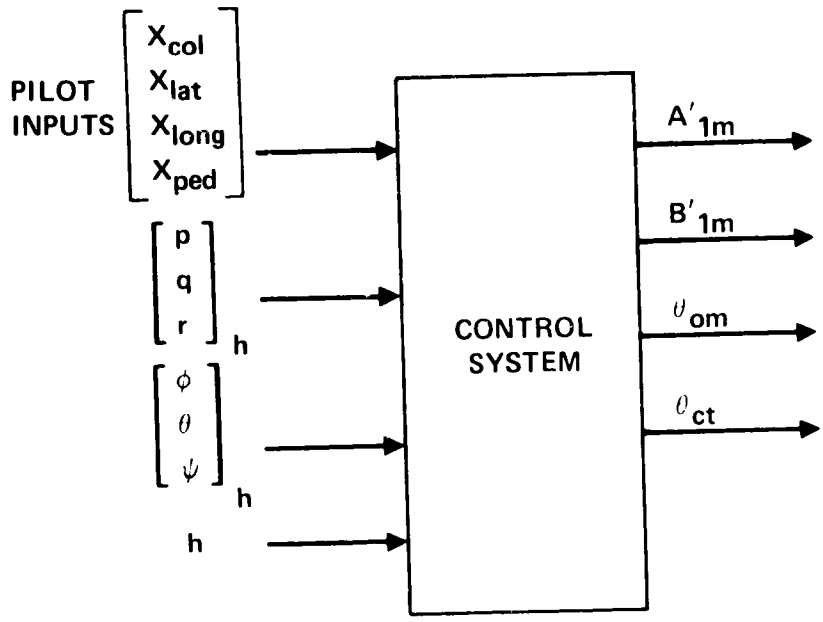

(f) Control system.

Figure 3.- Continued.

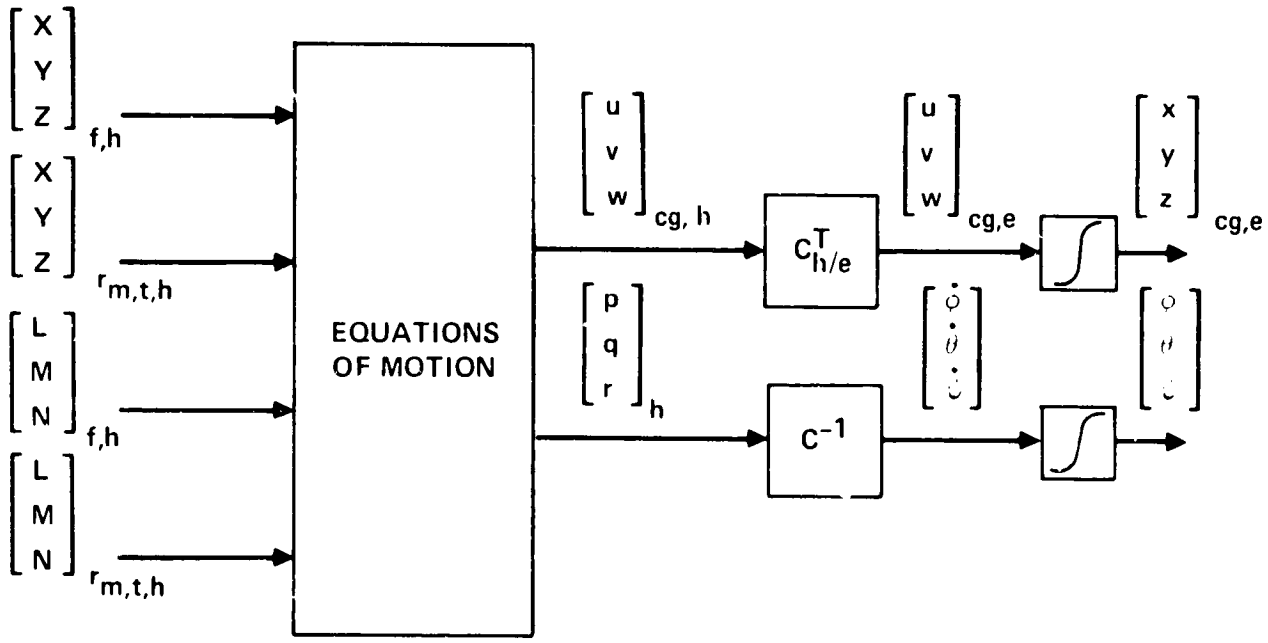

(g) Equations of motion.

Figure 3.- Concluded.

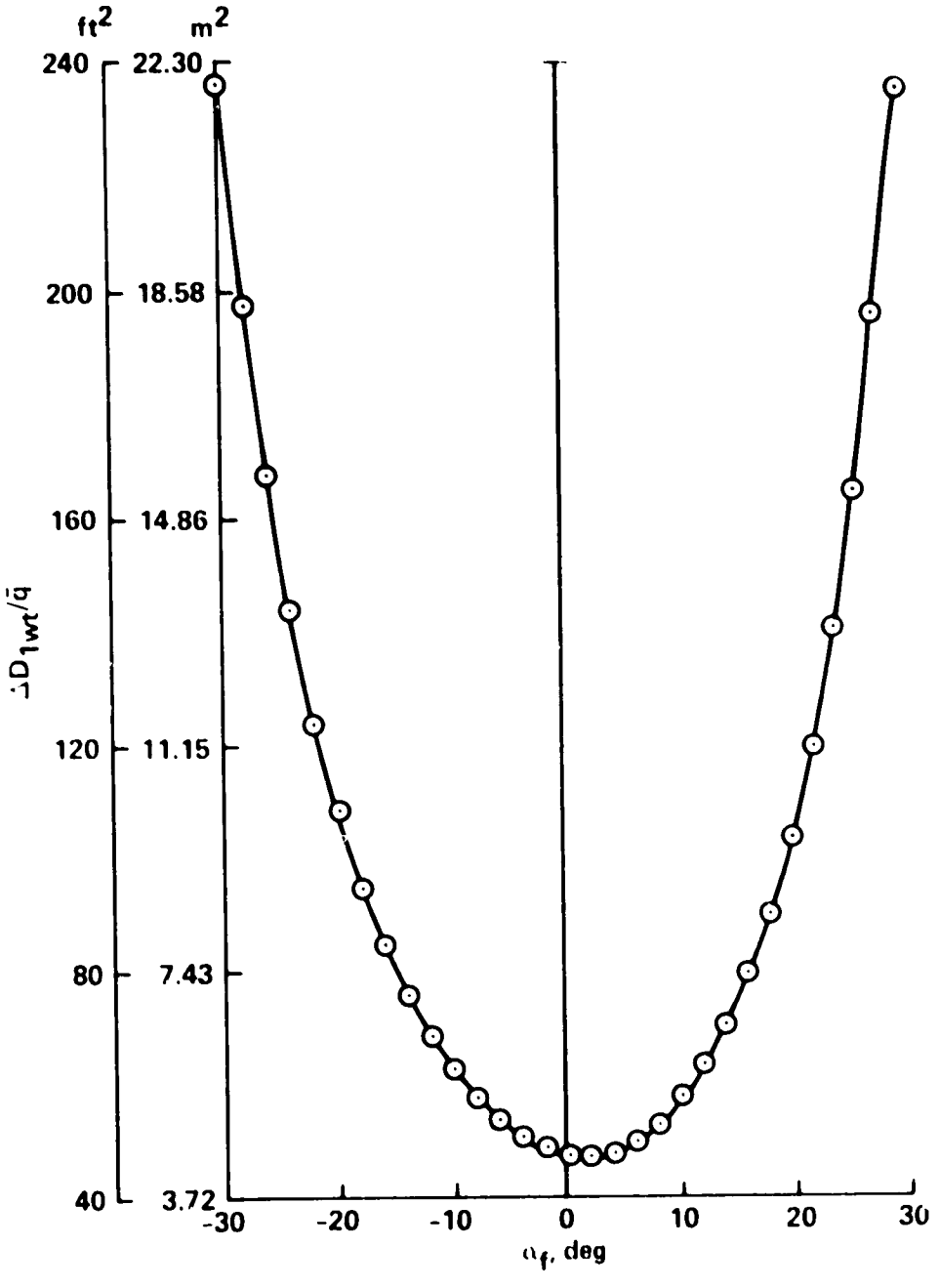

Figure 4.- Fuselage incremental drag as a function of angle of attack.

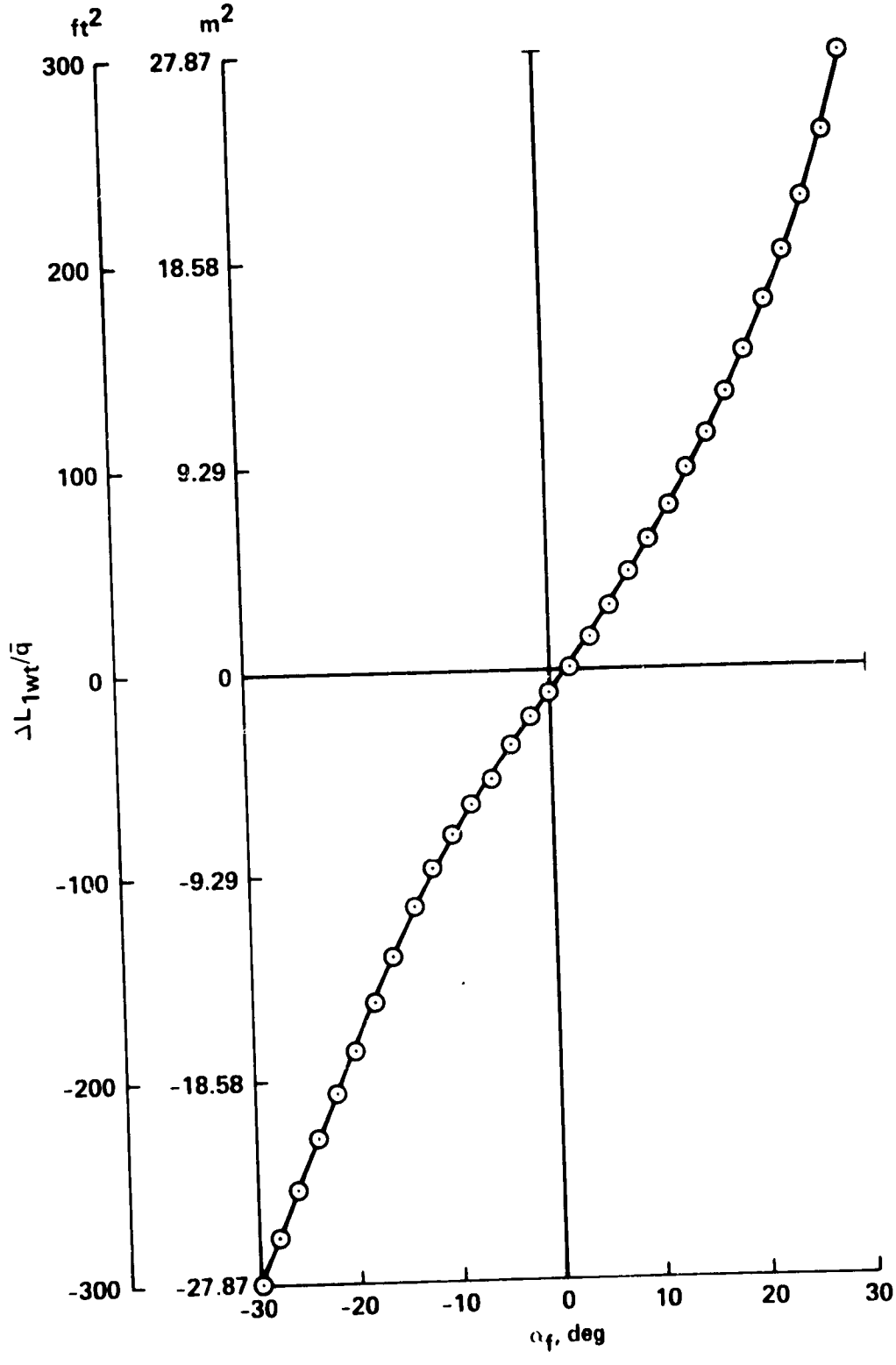

Figure 5.- Fuselage incremental lift as a function of angle of attack.

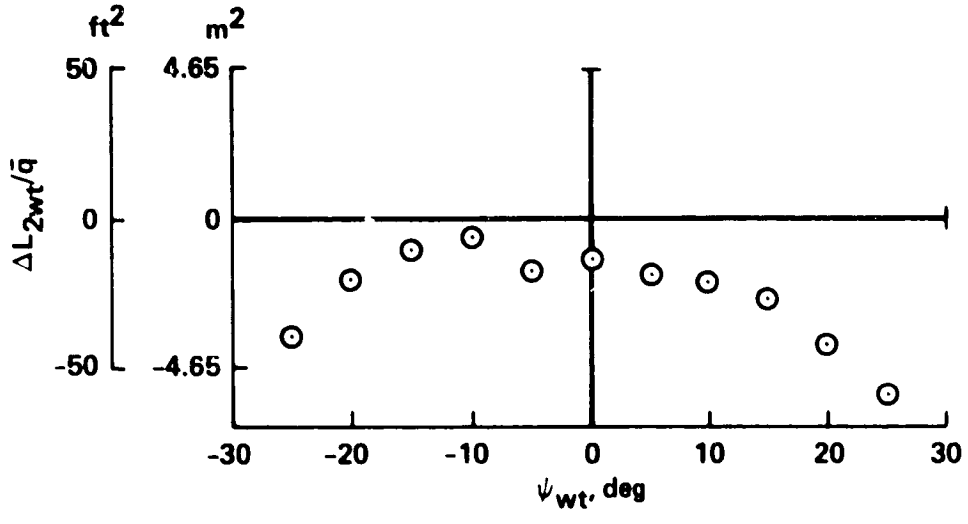

Figure 6.- Fuselage incremental lift as a function of sideslip (wind tunnel yaw angle).

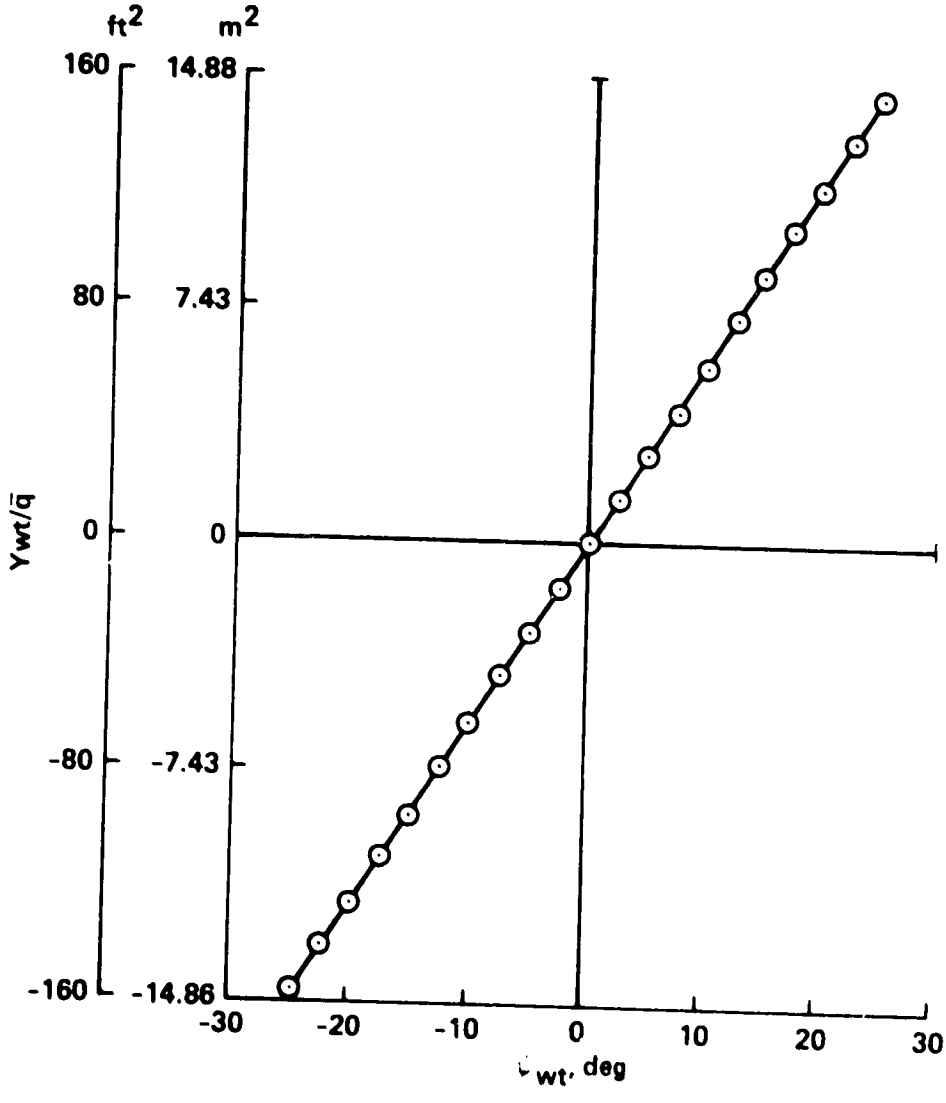

Figure 7.- Fuselage sideforce as a function of sideslip (wind tunnel yaw angle).

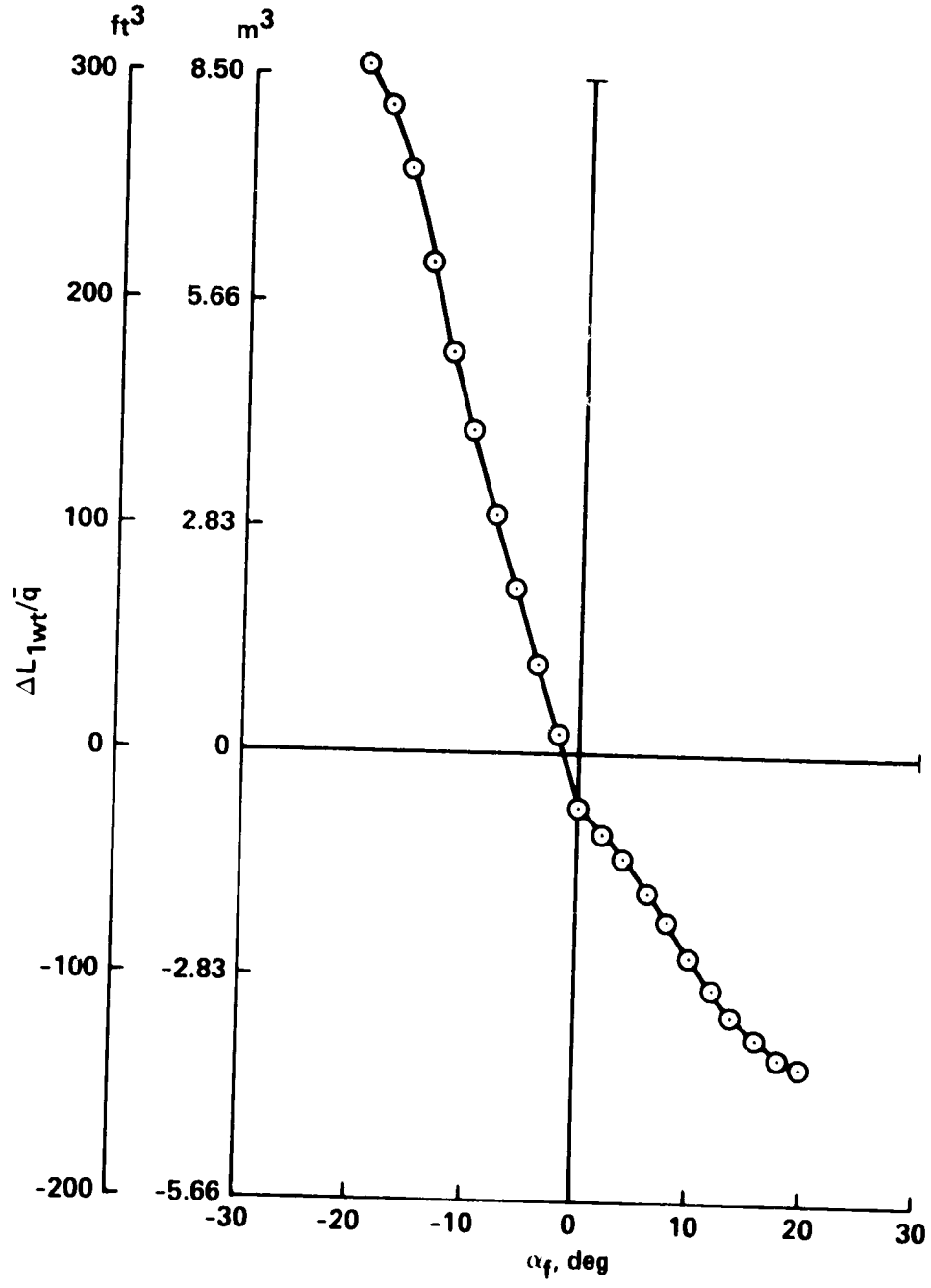

Figure 8.- Fuselage incremental rolling moment as a function of angle of attack.

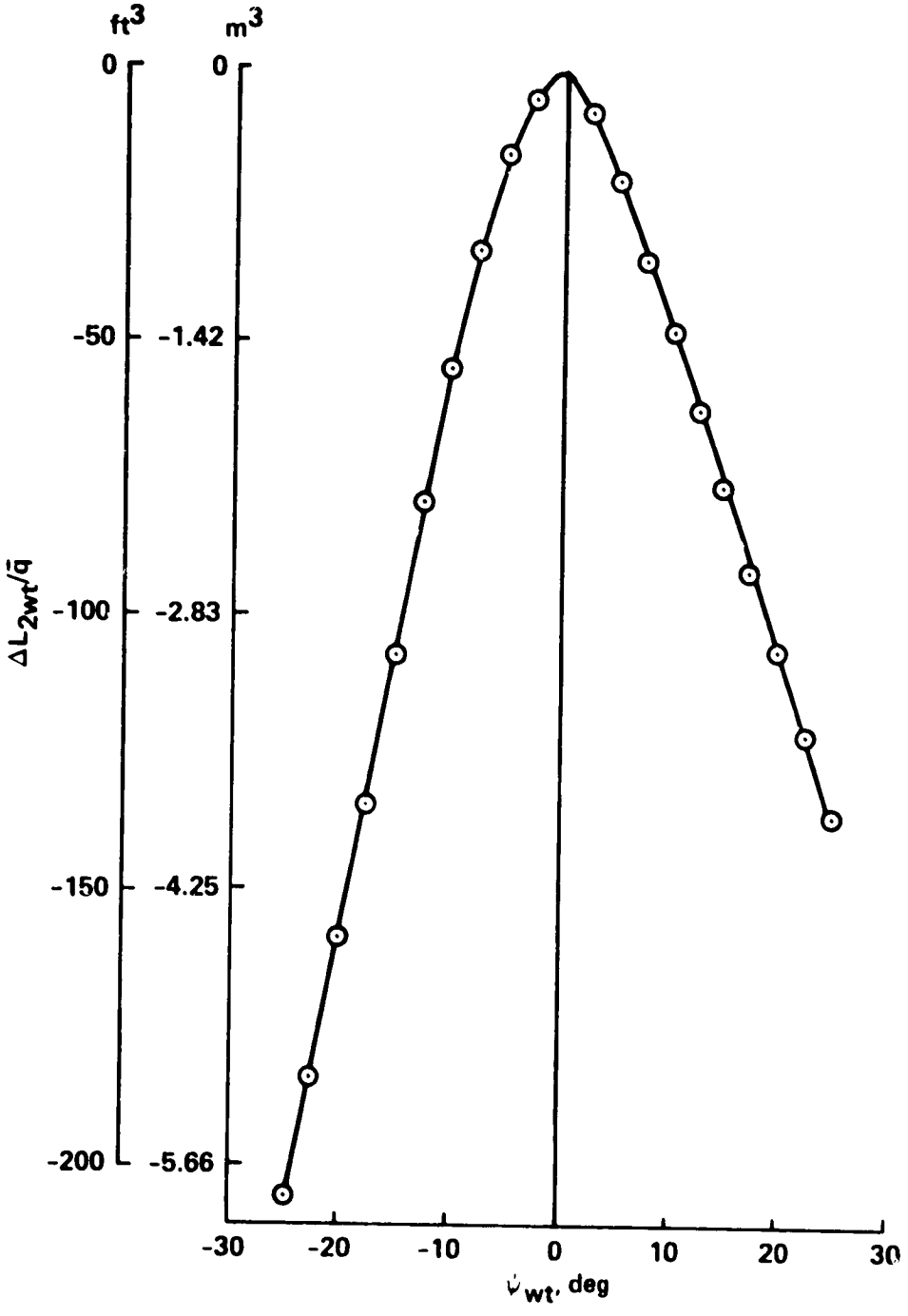

Figure 9.- Fuselage incremental rolling moment as a function of sideslip (wind tunnel yaw angle).

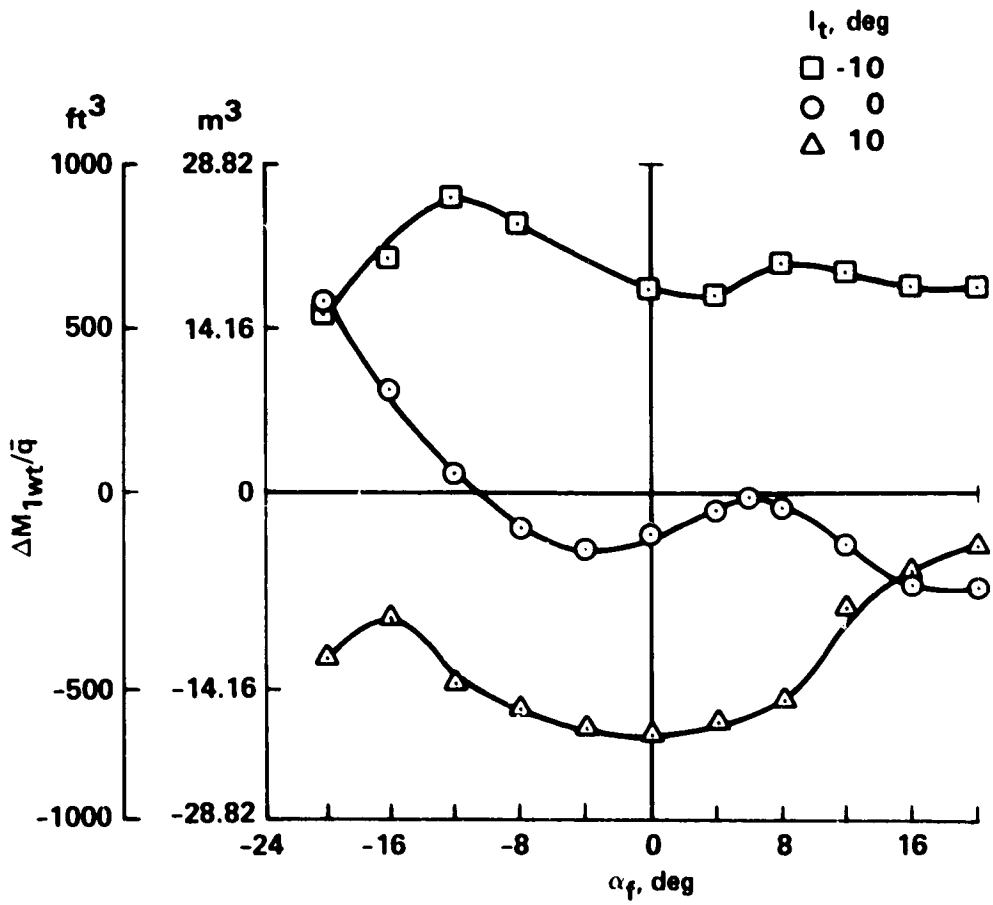

Figure 10.- Fuselage incremental pitching moment as a function of angle of attack and incidence at the tail.

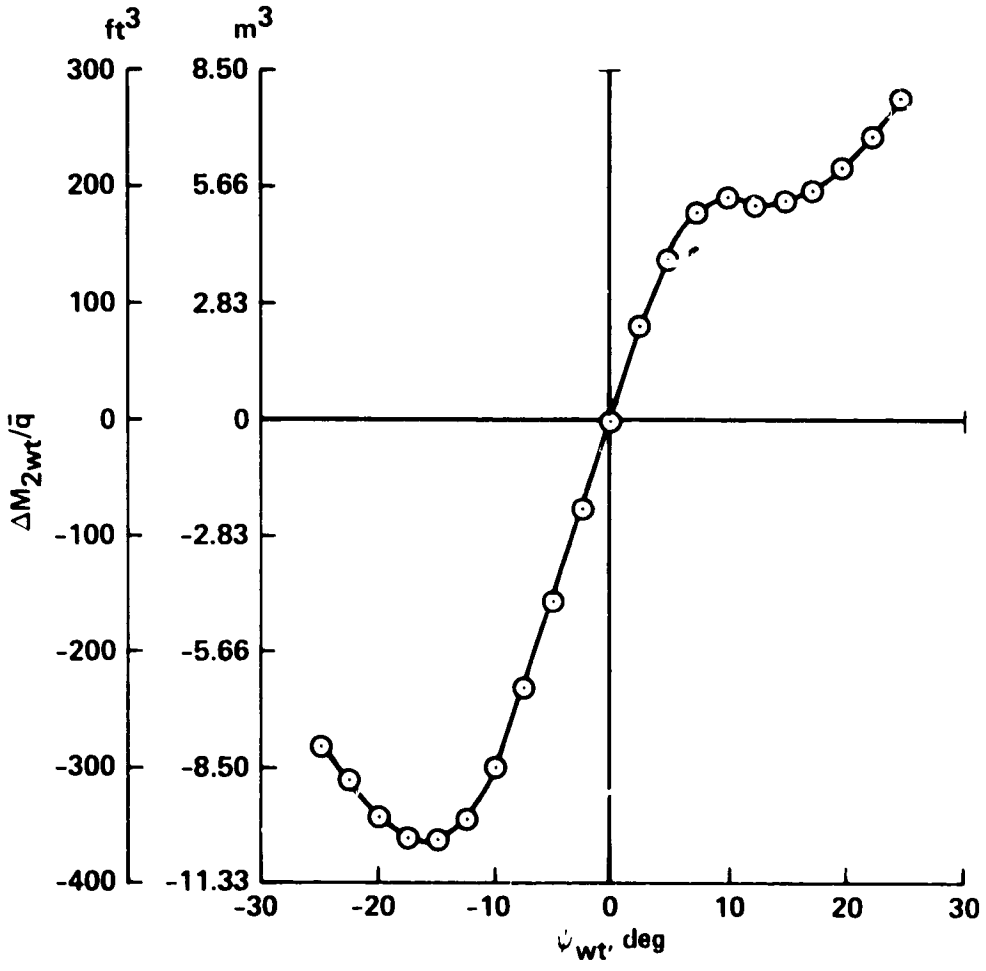

Figure 11.- Fuselage incremental pitching moment as a function of sideslip (wind tunnel yaw angle).

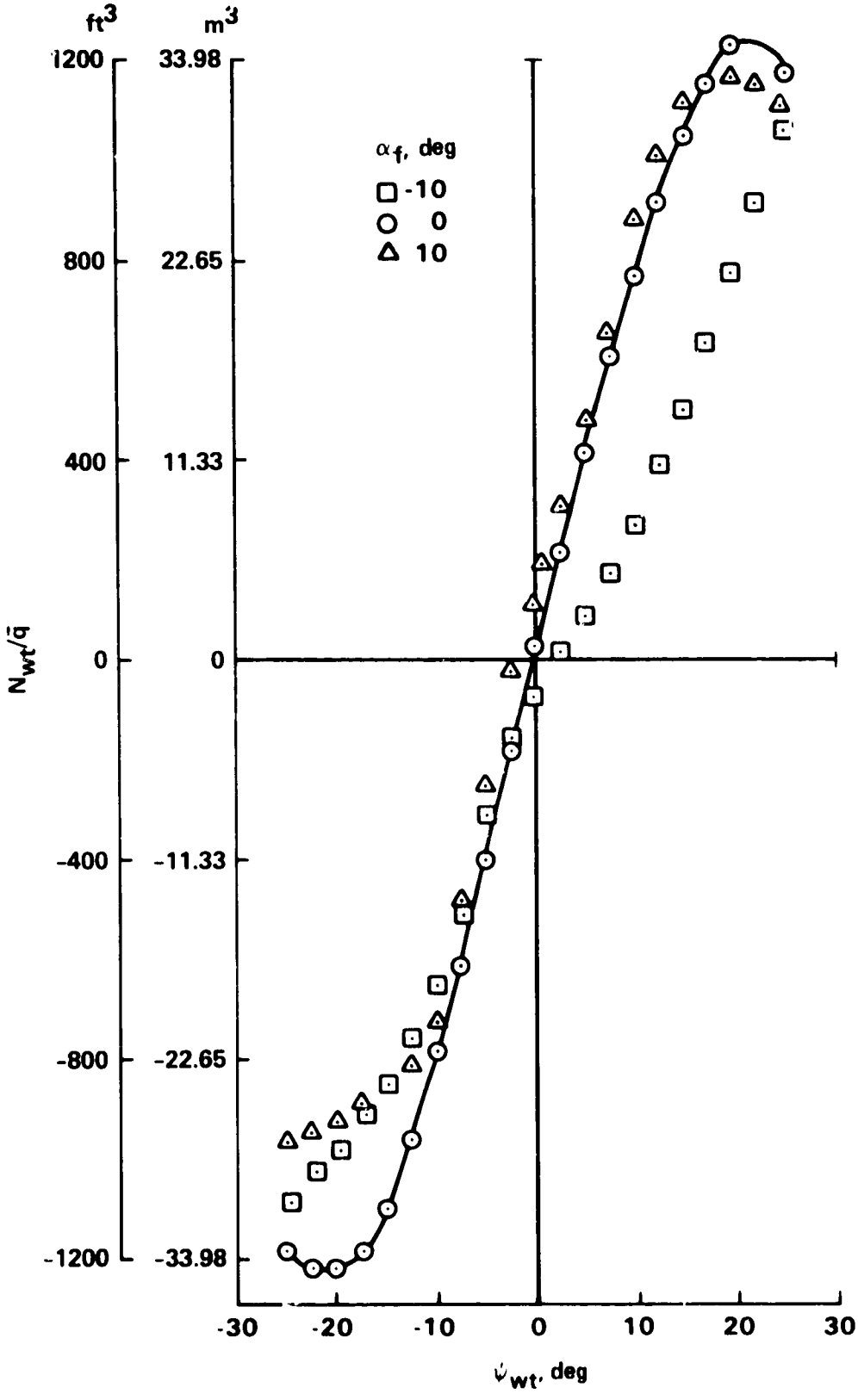

Figure 12.- Fuselage yawing moment as a function of sideslip (wind tunnel yaw angle) and angle of attack.

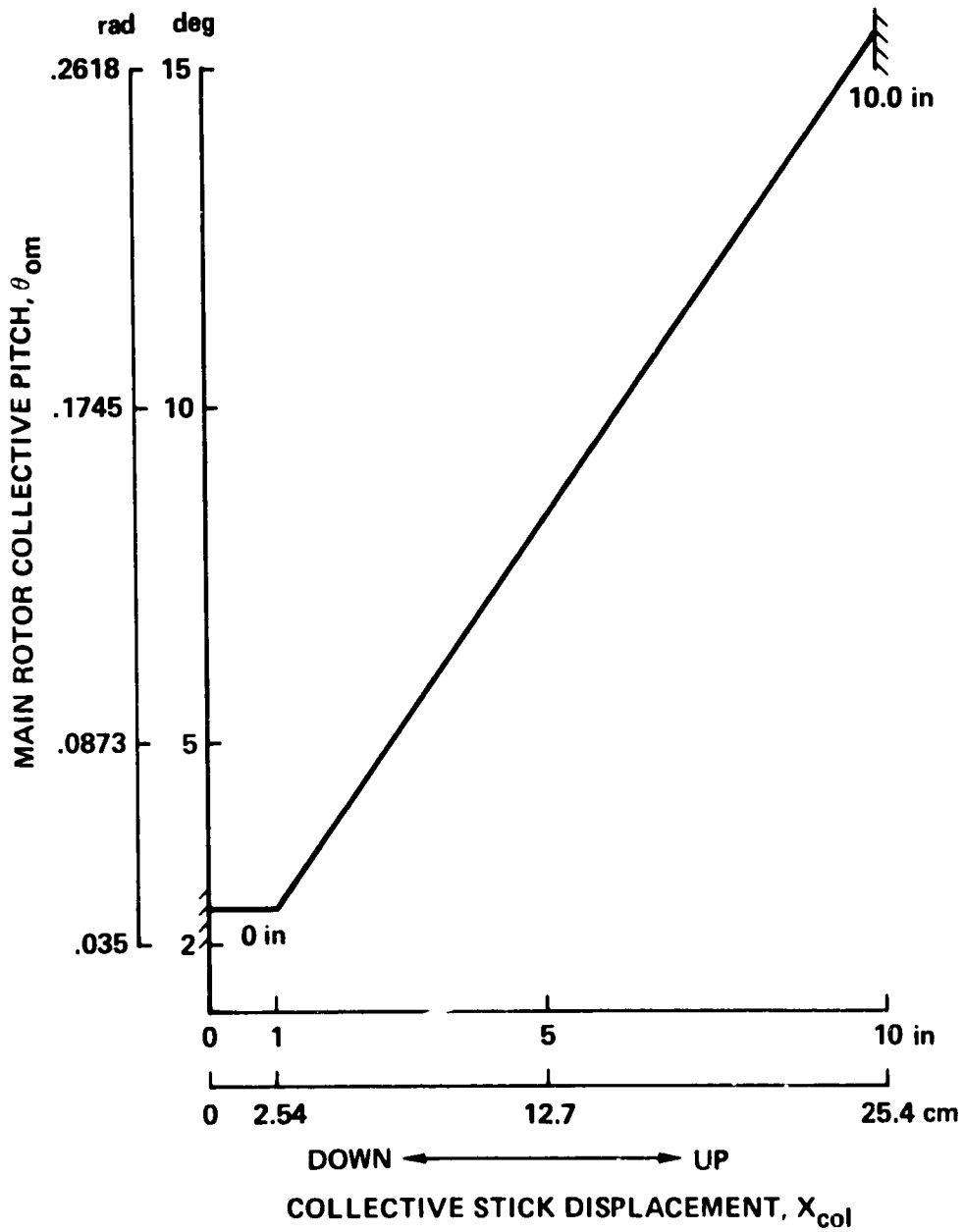

(a) Collective

Figure 13.- Control rigging diagrams.

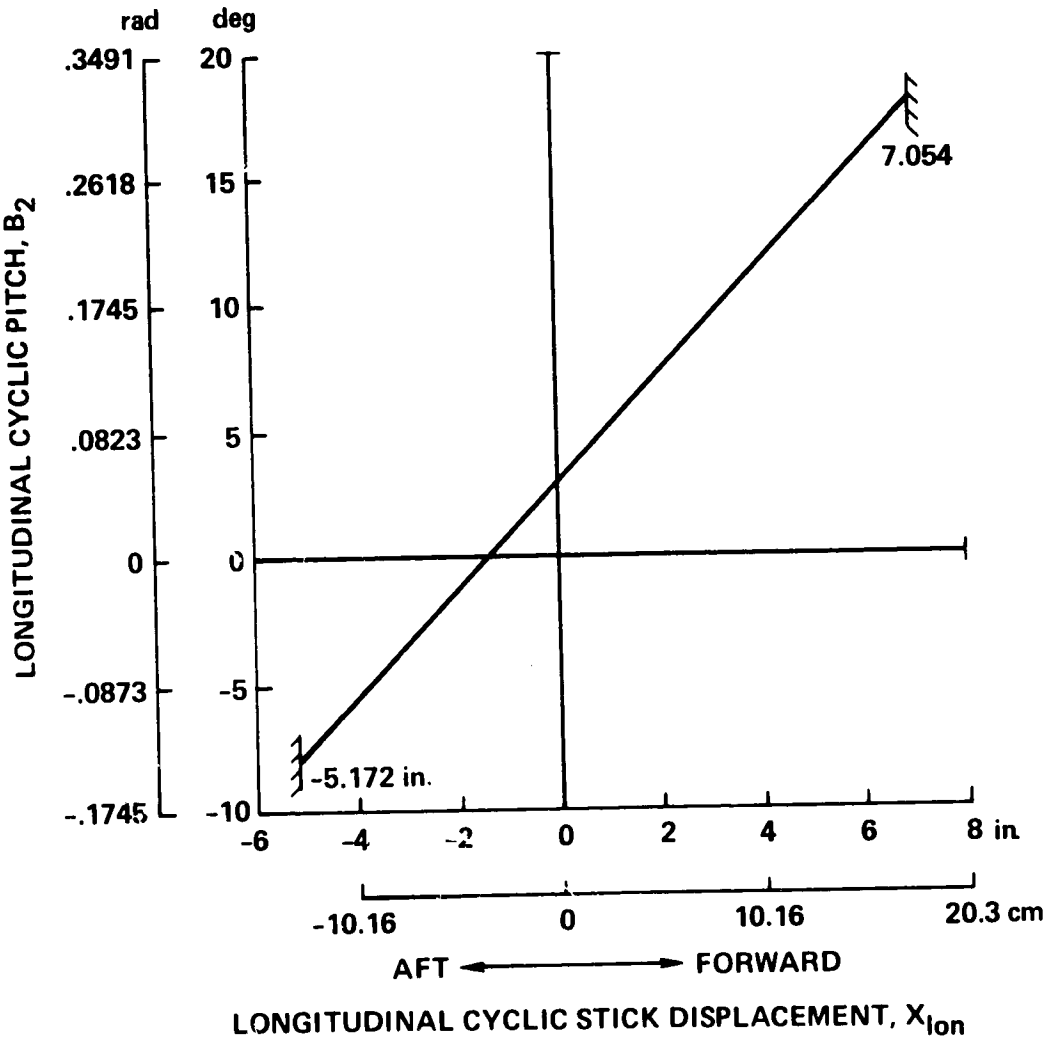

(b) Longitudinal cyclic

Figure 13.- Continued.

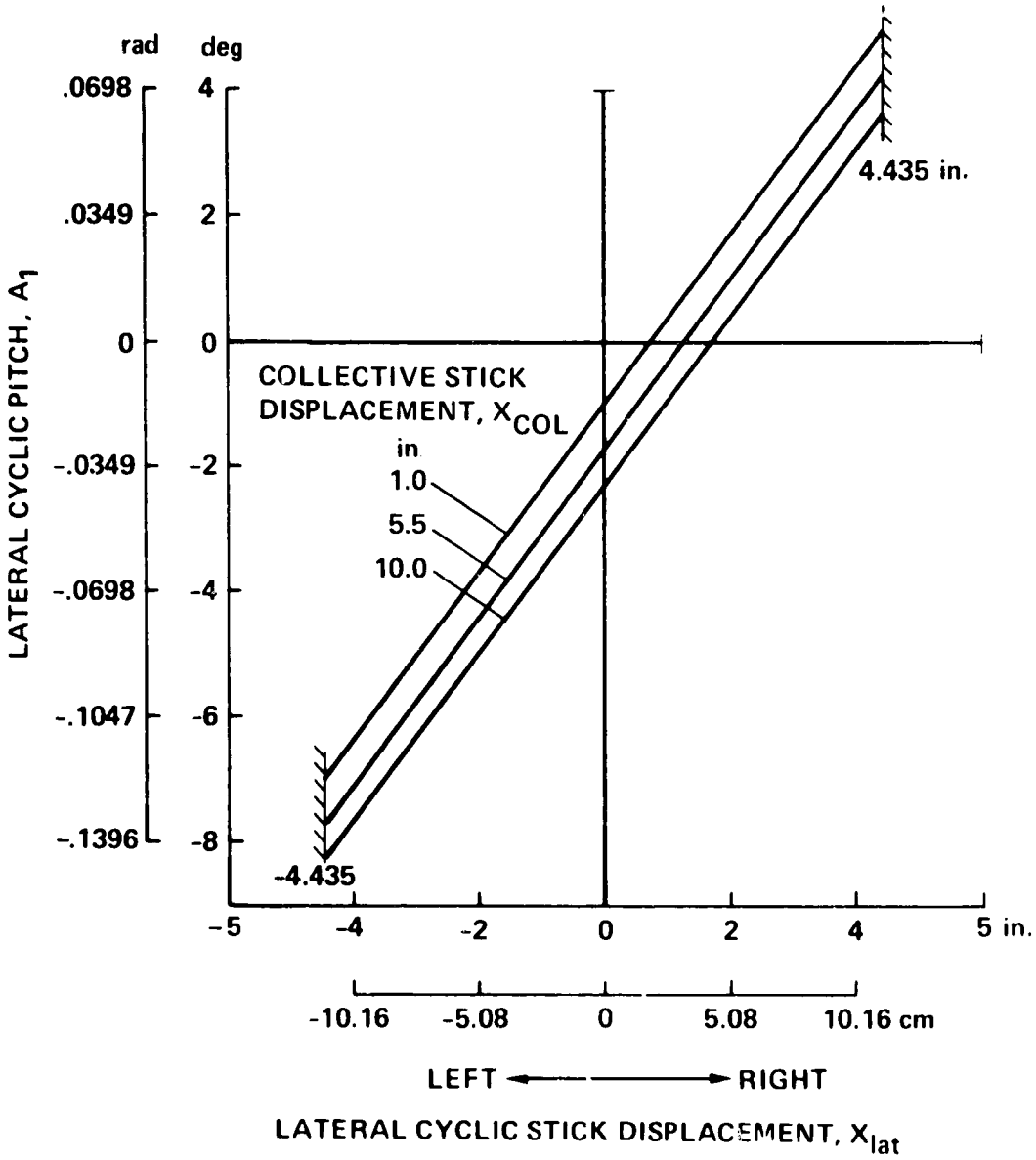

(c) Lateral cyclic

Figure 13.- Continued.

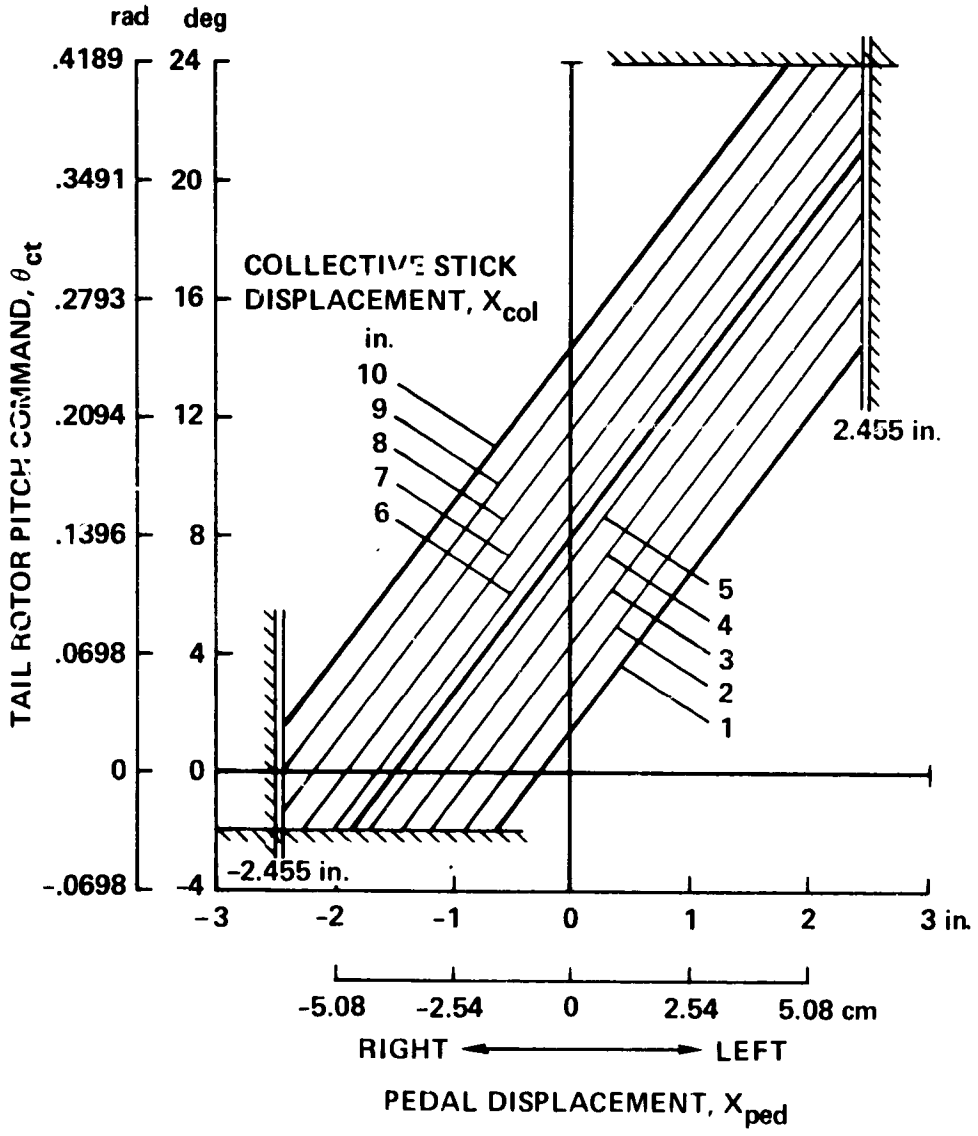

(d) Pedal

Figure 13.- Concluded.

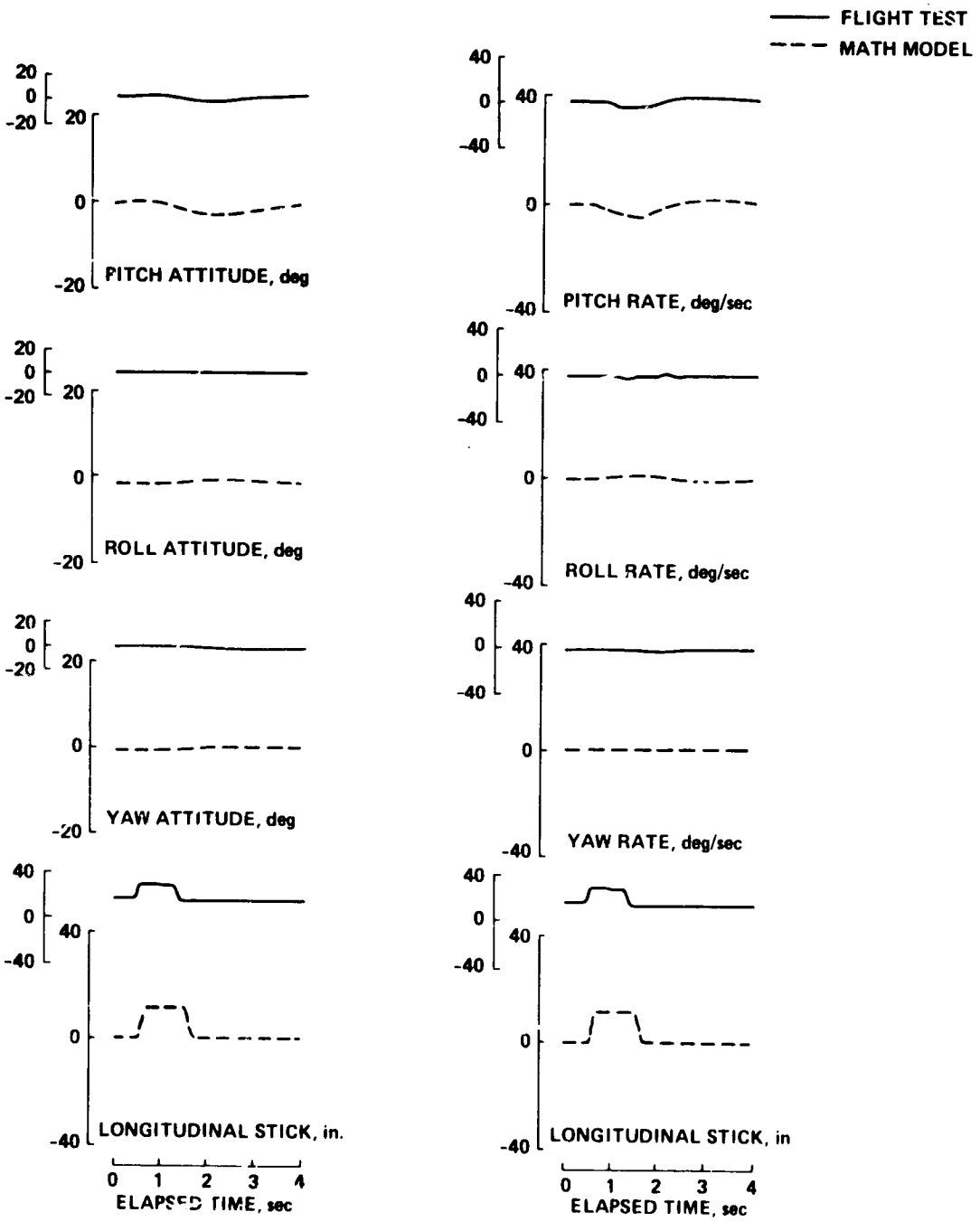

(a) Longitudinal cyclic pulse.

Figure 14.- Flight test-math model comparisons.

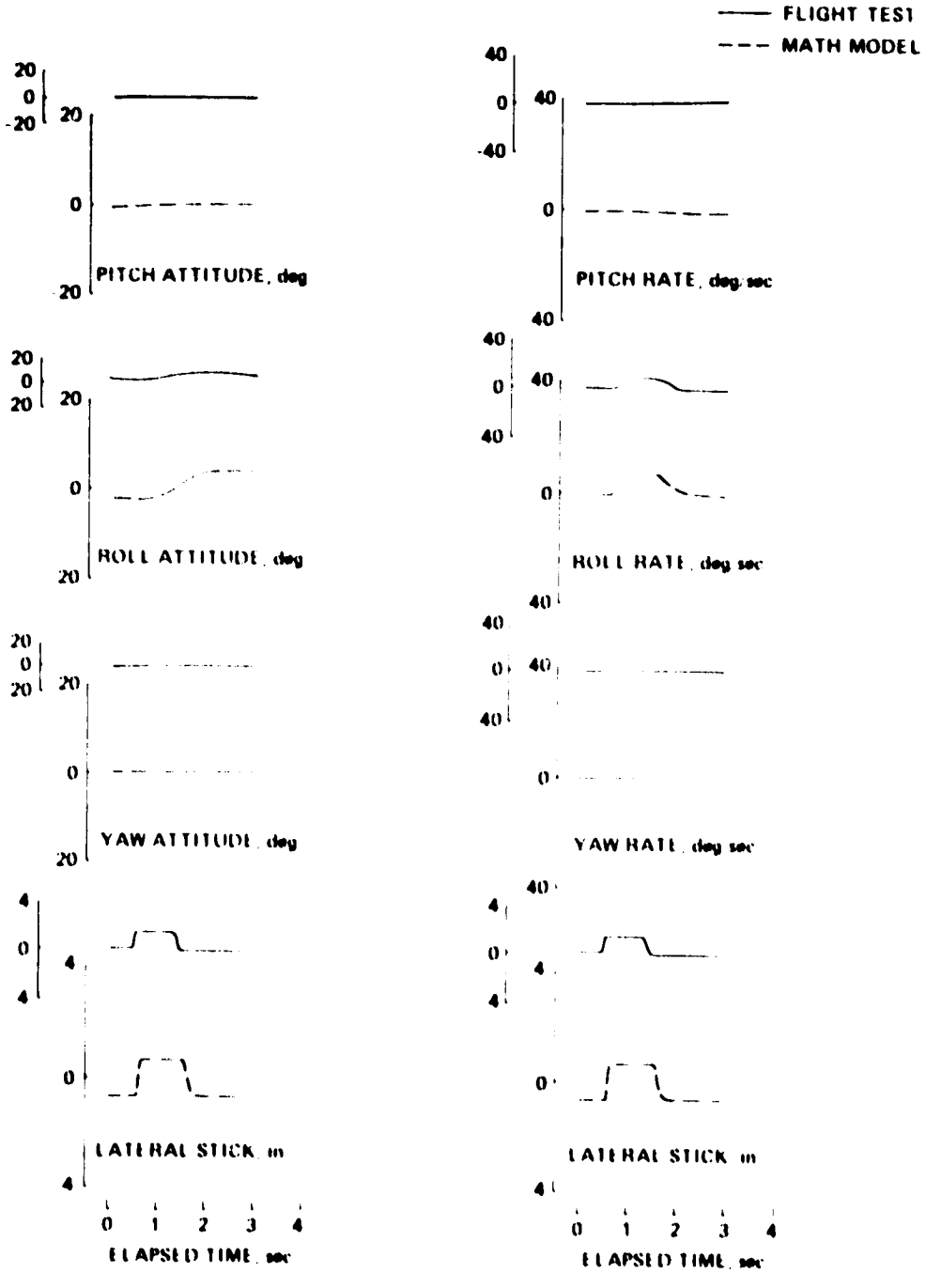

(b) Lateral cyclic pulse.

Figure 14. Continued.

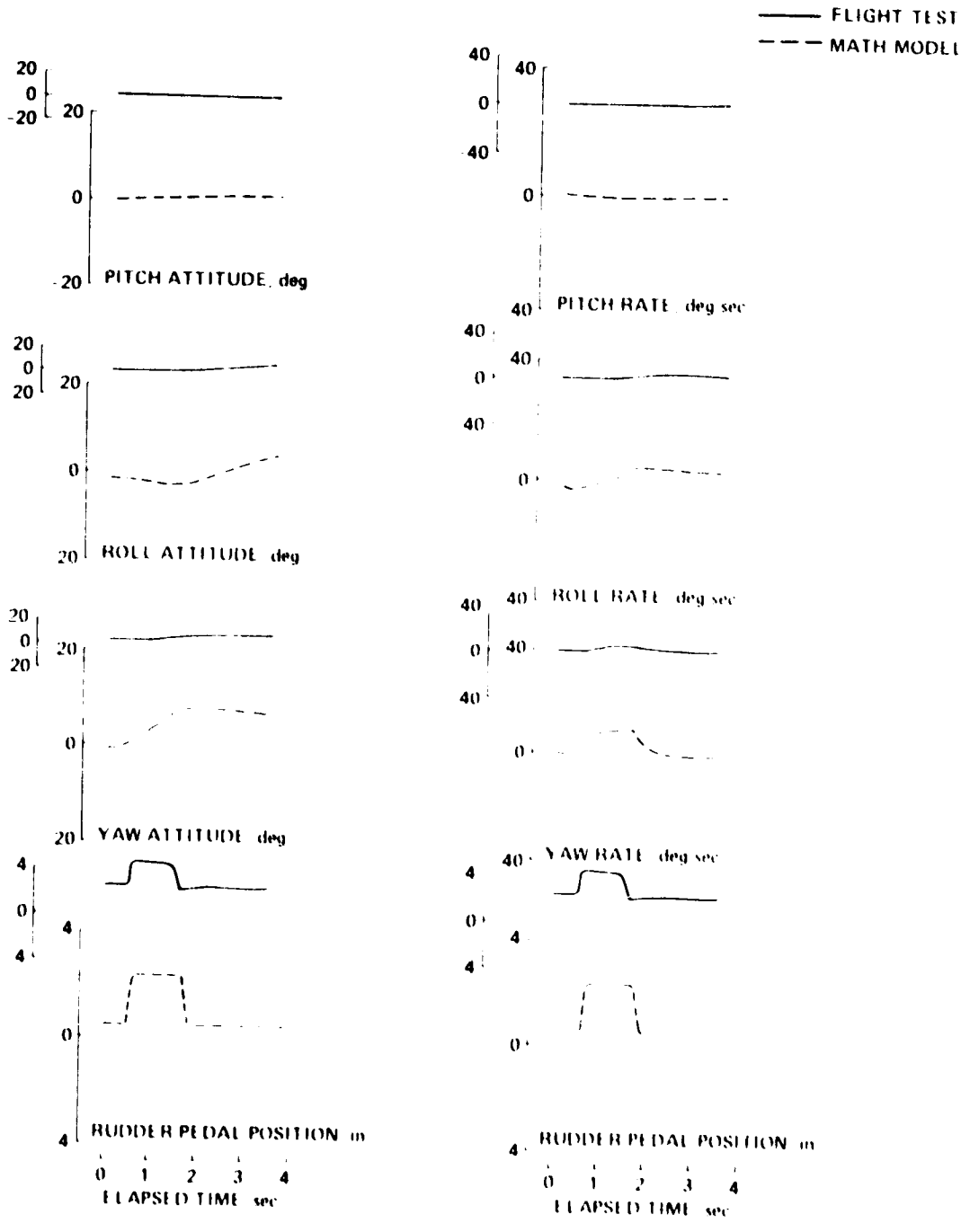

(c) Right directional pulse.

Figure 14. Concluded.